AD-A074 450 OHIO STATE UNIV COLUMBUS ELECTROSCIENCE LAB F/G 9/5
ANALYSIS OF WIRE ANTENNAS MOUNTED NEAR OR AT THE EDGE OF A HALF--ETC(U)
AUG 79 D M POZAR, E H NEWMAN DAAG29-76-G-0331
UNCLASSIFIED ESL-784569-9 ARO-14012.5-EL NL
/ OF /
AD
A074450

END
DATE
FILMED
10-79
DDC

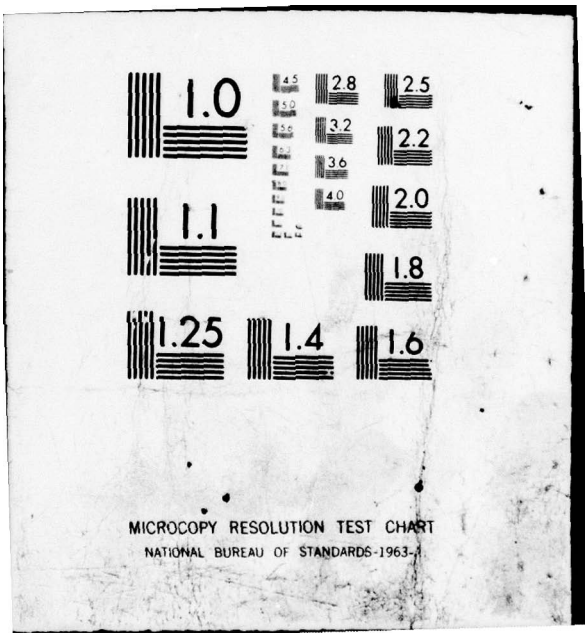
1.0
1.1
1.25
1.4
1.6
1.8
2.0
2.2
2.5
2.8
3.2
3.6
4.0
4.5
5.0
5.6
MICROCOPY RESOLUTION TEST CHART
NATIONAL BUREAU OF STANDARDS-1963-A

OSU

The Ohio State University

ANALYSIS OF WIRE ANTENNAS MOUNTED NEAR OR AT THE EDGE OF A HALF-PLANE

D. M. Pozar and E. H. Newman

The Ohio State University

ElectroScience Laboratory

Department of Electrical Engineering
Columbus, Ohio 43212

Technical Report 784569-9
Grant Number DAAG-76-G-0331
August 1979

Department of the Army
U. S. Army Research Office
Research Triangle Park, North Caroline 27709

SECURITY CLASSIFICATION OF THIS PAGE (When Data Entered)

REPORT DOCUMENTATION PAGE

READ INSTRUCTIONS BEFORE COMPLETING FORM

1. REPORT NUMBER
2. GOVT ACCESSION NO.
3. RECIPIENT'S CATALOG NUMBER

4. TITLE (and Subtitle)
(6) ANALYSIS OF WIRE ANTENNAS MOUNTED NEAR OR AT THE EDGE OF A HALF-PLANE.

5. TYPE OF REPORT & PERIOD COVERED
(9) Technical Report

6. PERFORMING ORG. REPORT NUMBER
(14) ESL-784569-9

7. AUTHOR(s)
(10) D. M. Pozar
E. H. Newman

8. CONTRACT OR GRANT NUMBER(s)
(15) Grant No. DAAG29-76-G-0331

9. PERFORMING ORGANIZATION NAME AND ADDRESS
The Ohio State University ElectroScience Laboratory
Department of Electrical Engineering
Columbus, Ohio 43212

10. PROGRAM ELEMENT, PROJECT, TASK AREA & WORK UNIT NUMBERS
(12) 51p.

11. CONTROLLING OFFICE NAME AND ADDRESS
Department of the Army
U. S. Army Research Office
Research Triangle Park, North Carolina 27709

(11) 12. REPORT DATE
August 1979

13. NUMBER OF PAGES
47

14. MONITORING AGENCY NAME & ADDRESS(if different from Controlling Office)
(18) ARO (19) 14012.5-EL

15. SECURITY CLASS. (of this report)
Unclassified

15a. DECLASSIFICATION/DOWNGRADING SCHEDULE

16. DISTRIBUTION STATEMENT (of this Report)

Approved for public release; distribution unlimited.

17. DISTRIBUTION STATEMENT (of the abstract entered in Block 20, if different from Report)

18. SUPPLEMENTARY NOTES

THE VIEW, OPINIONS, AND/OR FINDINGS CONTAINED IN THIS REPORT ARE THOSE OF THE AUTHOR(S) AND SHOULD NOT BE CONSTRUED AS AN OFFICIAL DEPARTMENT OF THE ARMY POSITION, POLICY, OR DECISION, UNLESS SO DESIGNATED BY OTHER DOCUMENTATION.

19. KEY WORDS (Continue on reverse side if necessary and identify by block number)

Antennas
Moment methods
Numerical techniques
Half-plane

lambda

20. ABSTRACT (Continue on reverse side if necessary and identify by block number)

The problem of a monopole antenna mounted near or at the edge of a half-plane is solved using a hybrid moment method solution with an integral expression for the exact half-plane Green's function, and by the MM/GTD method. Results are presented for input impedance of a $\lambda/4$ monopole vs. distance from the half-plane edge, and vs. angle for an edge-mounted antenna. Simple expressions for the surface current density induced on the half-

DD FORM 1 JAN 73 1473 EDITION OF 1 NOV 65 IS OBSOLETE

4/02 251

SECURITY CLASSIFICATION OF THIS PAGE (When Data Entered)

JOB 4

20.

plane are derived and used to synthesize an attachment mode for use with the author's previously developed surface patch moment method solution when a wire is attached at or near an edge of a finite plate.

CONTENTS

		Page
I.	INTRODUCTION	1
II.	SOLUTION FOR ANTENNA NEAR EDGE OF HALF-PLANE USING EXACT GREEN'S FUNCTION	2
	A. Method of Solution	3
	B. Formulation of MM/Green's Function Solution	5
	C. Results	11
	D. ϕ-variation of Wire Current	12
	E. Expressions for Surface Currents	15
III.	SOLUTION FOR MONOPOLE NEAR EDGE OF HALF-PLANE USING MM/GTD	23
	A. Formulation of MM/GTD Solution	23
	B. Comparison of Results from Sections II and III	24
IV.	SOLUTION FOR MONOPOLE MOUNTED AT THE EDGE OF A HALF-PLANE USING MM/GREEN'S FUNCTION	27
	A. Formulation of MM/Green's Function Solution	27
	B. Expression for Surface Current	31
V.	SURFACE PATCH MM SOLUTION	33
	A. Description of Attachment Mode Development	34
	B. Results and Comparisons with Solutions from Sections II, III, IV	40
VI.	CONCLUSION	43
REFERENCES		46

I. INTRODUCTION

A problem of continued interest is that of antennas mounted on finite conducting bodies. Antennas on spherical bodies have been analyzed[1], as well as antennas on more general structures[2,3]. The authors have previously[4] presented a surface patch moment method solution for geometries involving wires and rectangular plates, including wire/plate and plate/plate junctions. In that work, the wire attachment point was restricted to be 0.1λ or more from any plate edge. This report presents work which allows attachment points to be near or at a half-plane-type edge, and also serves as a start to the problem of wire attachments near the edge of two plates intersecting at an arbitrary angle (a wedge). Also presented are canonical solutions to the problem of a monopole near or at the edge of a perfectly conducting half-plane. These solutions are in terms of near field parameters, i.e., currents and input impedance. Far-field results for antennas near half-plane edges are available in [5].

Various types of solutions are presented for each of two related geometries: a vertical monopole near an edge and a radial monopole mounted on an edge. The first type of solution is a rigorous hybrid Green's function moment method solution for an antenna near or at the edge of a perfectly conducting half-plane. This solution uses an integral expression for the exact half-plane Green's function, with the source and image terms separated from the edge diffracted field. This procedure serves as an accurate canonical solution for comparison with other solutions. Other results of this solution are simple closed form expressions for the near zone surface currents for a source near or at an edge, which are later used to synthesize a surface patch moment method attachment mode. Different Green's functions are used depending on whether the antenna is near the edge or on the edge.

The second type of solution presented is similar to the first, except the GTD is used to find the diffracted field, rather than using the exact Green's function. This solution is essentially the MM/GTD hybrid method developed by Thiele and Newhouse[2]. Agreement with the MM/Green's function is good for vertical monopoles as close as $.2\lambda$ from the edge.

Since GTD is not accurate for source and field points both very near the edge, the MM/GTD solution was not carried out for radial monopoles mounted on an edge.

The third solution involved constructing a new expansion mode for wires attached near or at an edge, for use in the surface patch MM solution[4]. The new mode was based on the form of the surface currents found via the exact Green's function. Also, a special mode to enforce the proper edge singularity for the component of surface current parallel to the edge was developed. This mode was found to have practically no effect on the input impedance.

II. SOLUTION FOR ANTENNA NEAR EDGE OF HALF-PLANE USING EXACT GREEN'S FUNCTION

The problem of a wire antenna in free space can be solved via the moment method solution of an integral equation using the free space Green's function[6]. If the wire antenna is in the presence of another scattering structure there are two possible modifications. The first is to replace the free-space Green's function by the special Green's function for the particular scattering structure. The second approach is to retain the free-space Green's function, but suitably expand the currents on the wire and the scattering structure, and solve for the expansion coefficients in the MM solution. The advantage of the first approach is that no new unknowns are introduced into the MM solution and the size of the impedance matrix does not increase over that of the isolated wire, while the disadvantage is that the Green's function of the scatterer must be known in a computationally efficient form. The advantage of the second approach is that the Green's function of the scatterer need not be known, while the disadvantage is that new unknowns are introduced and the size of the required impedance matrix can increase substantially if the scatterer is electrically large.

The first approach is used in this section and in Sections III and IV, while the second approach is used in Section V.

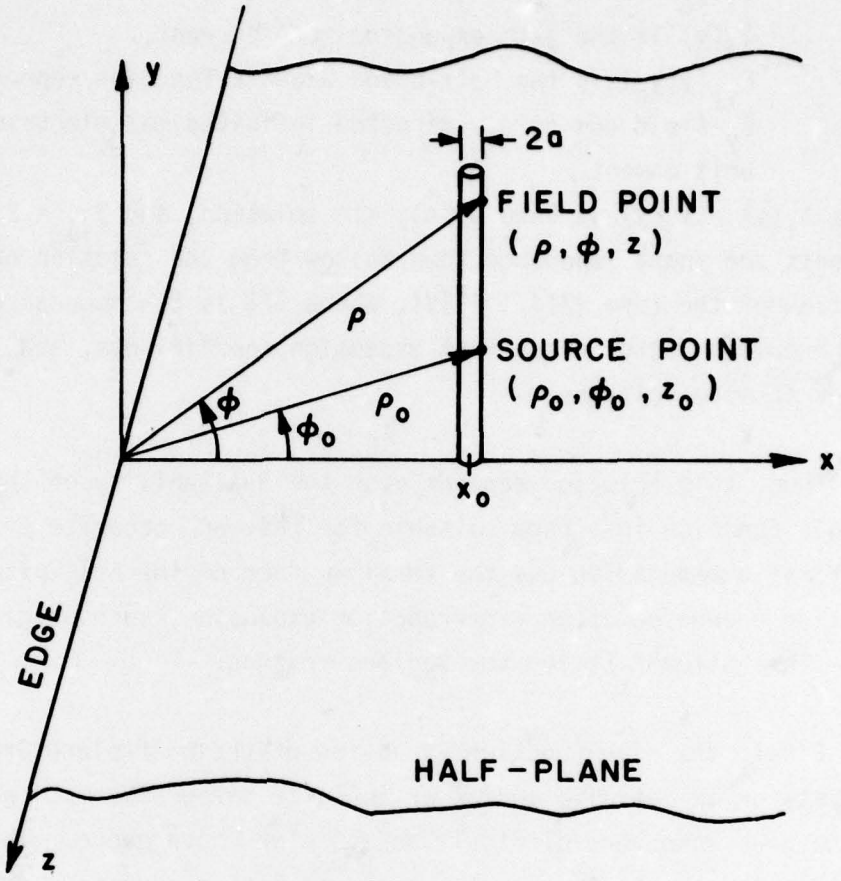

Figure 1. Geometry and coordinate systems for a vertical monopole near the edge of a half-plane.

A. Method of Solution

The geometry of the problem is shown in Figure 1. The wire and half-plane are for simplicity considered to be perfectly conducting. The basic idea of the solution is to expand the wire currents using piecewise-sinusoidal modes, find the fields of test modes (also PWS) in the presence of the half-plane, and compute an impedance matrix:

$$Z_{ij} = -\int_{y_j} I_j(y) \int_{y_i} I_i(y_0) E_{yy}(y|y_0)\, dy_0\, dy \qquad (1)$$

where $I_i(y_o)$ is the i-th test mode current,
$I_j(y)$ is the j-th expansion mode current,
and $E_{yy}(y|y_o)$ is the half-plane Green's function representing the E_y field due to a y directed infinitesimal electric dipole of unit moment.

Since $I_i(y) = I_j(y)$ we have a Galerkin solution, and $Z_{ij} = Z_{ji}$. The wire currents and input impedance then follow from the solution of a matrix equation of the form [Z][I] = [V], where [Z] is the impedance matrix, [I] is the column vector of current expansion coefficients, and [V] is the vector of mode voltages.

Thus, this solution depends upon the availability of the half-plane Green's function in a form suitable for fast and accurate evaluation. It was first attempted to use the familiar form of the half-plane Green's function expressed as an eigenfunction expansion, such as given by Tai [5]. This attempt failed for various reasons.

First, the eigenfunction expansion of the half-plane Green's function consists of an infinite series of infinite integrals, making evaluation in the near zone very difficult due to slow convergence. The slow convergence is due to the fact that the eigenfunction expansion contains the singularities for the source and image terms. It was found that the source (or incident) terms could be subtracted off, and expressed in simple closed form, however, the authors were not able to do the same for the image (or reflected) field. Thus, the evaluation of self or overlapping mutual impedance terms would have been very difficult to do accurately. Also, the eigenfunction solution did not lend itself to small argument approximations for evaluation of near zone surface currents in simple closed form. It was found that the first term of the infinite series would give the correct edge behavior, but not the correct source singularity; the entire series was needed for that. For these reasons another type of solution for the half-plane Green's function was sought.

In 1953, Senior [7] gave the solution for diffraction of a vertical electric dipole by a half-plane. His solution was expressed in terms of derivatives of the scalar diffraction solution, which was expressed in integral form. As will be seen, this solution overcomes the problems which were met with the eigenfunction solution.

B. Formulation of MM/Green's Function Solution

For a vertical infinitesimal electric dipole of moment $I\ell$ in the presence of a conducting half-plane, the total field can be written as [7] (for $e^{j\omega t}$ time dependence):

$$E_y = \frac{I\ell Z_o}{4\pi j}\left\{\frac{-jk}{\sqrt{\rho\rho_o}}\cos\frac{\phi}{2}\cos\frac{\phi_o}{2}H_o^{(2)}(kR_1) + \frac{j}{2}\left(\frac{\partial^2}{\partial y\partial y_o} - k^2\right)I_R - \frac{j}{2}\left(\frac{\partial^2}{\partial y\partial y_o} + k^2\right)I_R'\right\} \tag{2}$$

$$H_x = \frac{I\ell}{4\pi j}\left\{\frac{k(z-z_o)}{R_1\sqrt{\rho\rho_o}}\cos\frac{\phi}{2}\cos\frac{\phi_o}{2}H_1^{(2)}(kR_1) + \frac{k}{2}\frac{\partial I_R}{\partial z_o} + \frac{k}{2}\frac{\partial I_{R'}}{\partial z_o}\right\} \tag{3}$$

$$H_z = \frac{I\ell}{4\pi j}\left\{\frac{-k}{2}\frac{\partial I_R}{\partial x_o} - \frac{k}{2}\frac{\partial I_{R'}}{\partial x_o}\right\} \tag{4}$$

where

$$I_R = \int_{-\mu_R}^{\infty} H_1^{(2)}(kR\cosh u)\,du \tag{5a}$$

and

$$I_{R'} = \int_{-\mu_{R'}}^{\infty} H_1^{(2)}(kR'\cosh u)\,du \tag{5b}$$

$$\mu_R = \sinh^{-1}\left\{\frac{2\sqrt{\rho\rho_o}}{R}\cos\frac{1}{2}(\phi-\phi_o)\right\}$$

$$\mu_{R'} = \sinh^{-1}\left\{\frac{2\sqrt{\rho\rho_0}}{R'}\cos\frac{1}{2}(\phi+\phi_0)\right\}$$

$$R = \sqrt{\rho^2+\rho_0^2-2\rho\rho_0\cos(\phi-\phi_0)+(z-z_0)^2} = \sqrt{(x-x_0)^2+(y-y_0)^2+(z-z_0)^2}$$

$$R' = \sqrt{\rho^2+\rho_0^2-2\rho\rho_0\cos(\phi+\phi_0)+(z-z_0)^2} = \sqrt{(x-x_0)^2+(y+y_0)^2+(z-z_0)^2}$$

$$R_1 = \sqrt{(\rho+\rho_0)^2+(z-z_0)^2}$$

$$Z_0 = 377\Omega.$$

The other field components (E_x,E_z,H_y) are not needed in this study but can be obtained from [7].

The incident and reflected electric fields can be written in terms of a Hertz potential:

$$E_y^{inc} = \frac{I\ell Z_0}{4\pi j}\left(\frac{\partial^2}{\partial y^2}+k^2\right)\frac{e^{-jkR}}{kR} \tag{6a}$$

$$E_y^{ref} = \frac{I\ell Z_0}{4\pi j}\left(\frac{\partial^2}{\partial y^2}+k^2\right)\frac{e^{-jkR'}}{kR'} \tag{6b}$$

Using the relation [7],

$$\int_{-\infty}^{\infty} H_1^{(2)}(kR\cosh u)du = 2j\frac{e^{-jkR}}{kR}, \tag{7}$$

in (5) gives

$$I_R = 2j\frac{e^{-jkR}}{kR} - \int_{\mu_R}^{\infty} H_1^{(2)}(kR\cosh u)du,$$

$$I_{R'} = 2j\frac{e^{-jkR'}}{kR'} - \int_{\mu_{R'}}^{\infty} H_1^{(2)}(kR'\cosh u)du. \tag{8}$$

Since $\frac{\partial R}{\partial y_o} = -\frac{\partial R}{\partial y}$ and $\frac{\partial R'}{\partial y_o} = \frac{\partial R'}{\partial y}$, (2) can be written as

$$E_y = \frac{I\ell Z_o}{4\pi j}\left\{\frac{-jk}{\sqrt{\rho\rho_o}}\cos\frac{\phi}{2}\cos\frac{\phi_o}{2}H_o^{(2)}(kR_1) + \left(\frac{\partial^2}{\partial y^2}+k^2\right)\frac{e^{-jkR}}{kR} - \left(\frac{\partial^2}{\partial y\partial y_o}-k^2\right)\pi^{dR}\right.$$

$$\left. + \left(\frac{\partial^2}{\partial y^2}+k^2\right)\frac{e^{-jkR'}}{kR'} + \left(\frac{\partial^2}{\partial y\partial y_o}+k^2\right)\pi^{dR'}\right\} \qquad (9)$$

where we have defined

$$\pi^{dR} = \frac{j}{2}\int_{\mu_R}^{\infty} H_1^{(2)}(kR\cosh u)du; \qquad (10a)$$

$$\pi^{dR'} = \frac{j}{2}\int_{\mu_{R'}}^{\infty} H_1^{(2)}(kR'\cosh u)du \qquad (10b)$$

Note that, using (7), π^{dR} and $\pi^{dR'}$ can be expressed in terms of a finite integral:

$$\pi^{dR} = -\frac{1}{2}\frac{e^{-jkR}}{kR} - \frac{j}{2}\int_0^{\mu_R} H_1^{(2)}(kR\cosh u)du, \qquad (11a)$$

$$\pi^{dR'} = -\frac{1}{2}\frac{e^{-jkR'}}{kR'} - \frac{j}{2}\int_0^{\mu_{R'}} H_1^{(2)}(kR'\cosh u)du. \qquad (11b)$$

It can be shown that π^{dR} and $\pi^{dR'}$ are not singular at R=0 or R'=0.

The geometrical optics (incident and reflected) fields can now be easily recognized, via (6), and separated from the diffracted field:

$$E_y = E_y^{inc} + E_y^{ref} + E_y^{dif} = E_y^{g.o.} + E_y^{dif} \tag{12}$$

$$E_y^{dif} = \frac{I\ell Z_o}{4\pi j}\left\{\frac{-jk}{\sqrt{\rho\rho_o}}\cos\frac{\phi}{2}\cos\frac{\phi_o}{2}H_o^{(2)}(kR_1) - \left(\frac{\partial^2}{\partial y\partial y_o} - k^2\right)\pi^{dR}\right.$$

$$\left. + \left(\frac{\partial^2}{\partial y\partial y_o} + k^2\right)\pi^{dR'}\right\} \tag{13}$$

The diffracted electric field is now in a form which has no singularities at the source or image.

Since the geometrical optics terms have been separated from the diffracted field, the impedance matrix [Z] can, for computational purposes, be broken into two parts; $[Z] = [Z_o] + [\Delta Z]$, where $[Z_o]$ represents the impedance matrix of a monopole on an infinite ground plane ($E_y^{g.o.}$ contribution) and $[\Delta Z]$ represents the E_y^{dif} field contribution which accounts for the edge. If PWS modes are used for expansion and testing the $[Z_o]$ elements can be computed in closed form using Richmond's subroutines [8], eliminating the difficulties which would be encountered if this evaluation were done numerically. This is an important and useful distinction from other similar solutions[1]. The remaining task is to evaluate $[\Delta Z]$.

The PWS modes are arranged on the wire as shown in Figure 2a, numbered from top to bottom. The test modes are positioned on the wire axis (at x_o, z_o=0) while the expansion modes are placed on the wire surface at (x ,z =a), where a is the wire radius. Note that the modes are PWS dipoles except for the bottom mode, which is a PWS monopole with its terminal at the base of the wire. This allows non-zero current at the attachment point. Figure 2b shows a typical test and expansion monopole, with coordinates, which make up the PWS modes. All segments are chosen with the same length, $d = |e_2-e_1| = |t_2-t_1|$. The current on the monopoles shown in Figure 2b can be written as

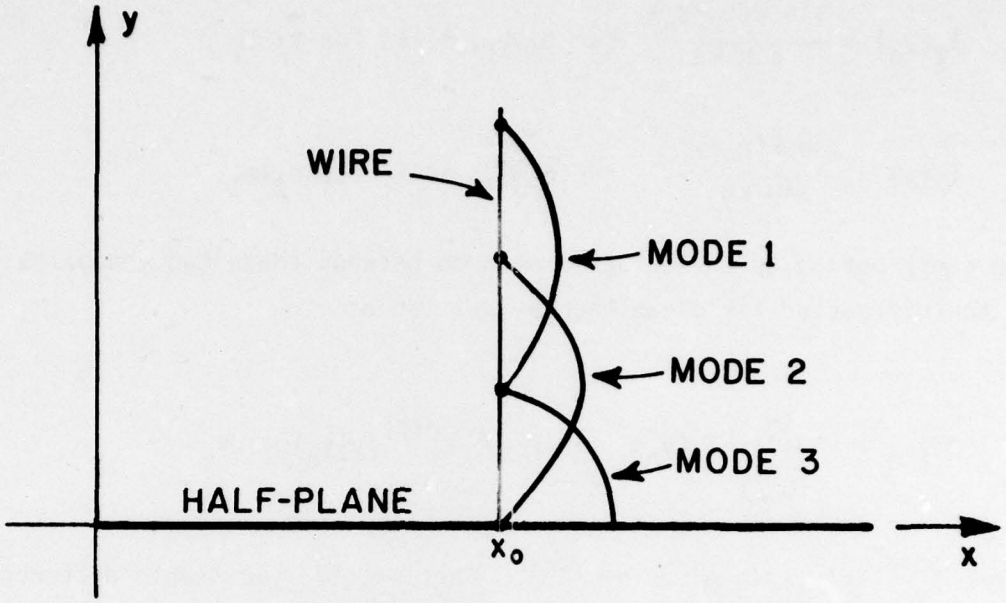

Figure 2a. PWS expansion mode arrangement on wire.

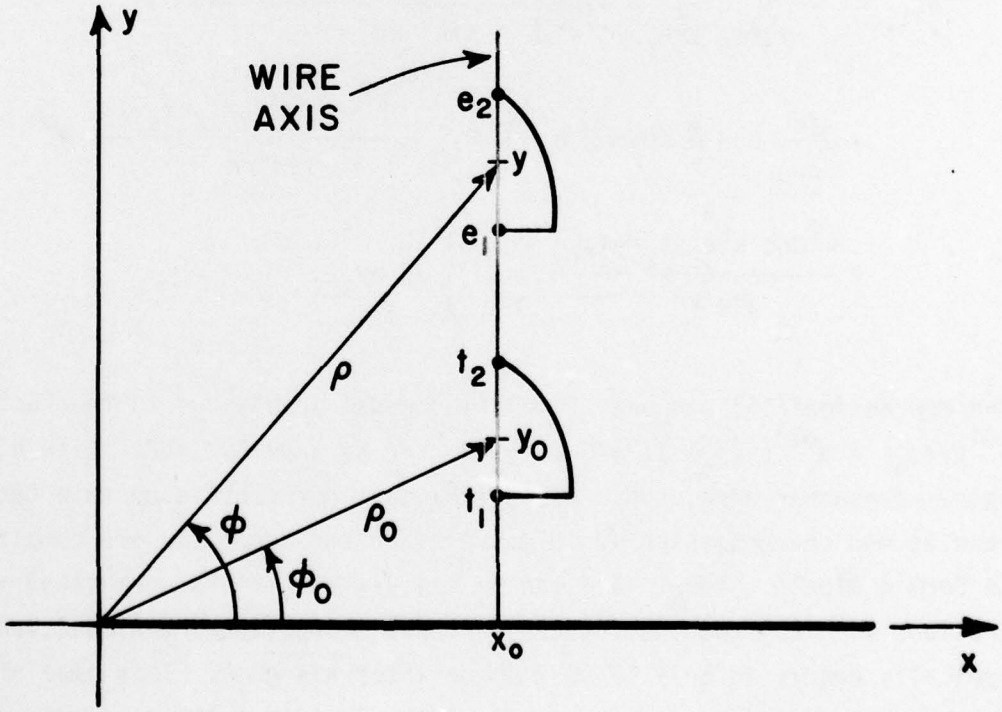

Figure 2b. Typical test and expansion monopoles and coordinates.

$$I_t(y_o) = \frac{\sin k(t_2-y_o)}{\sin kd} \quad \text{for } t_2 > t_1, \ *(-1) \text{ for } t_2 < t_1$$

$$I_e(y) = \frac{\sin k(e_2-y)}{\sin kd} \quad \text{for } e_2 > e_1, \ *(-1) \text{ for } e_2 < e_1.$$

The contribution to the mutual impedance between these two monopoles due to the diffracted field can then be written as

$$\Delta Z_{t,e} = - \int_{y_0=t_1}^{t_2} I_t(y_o) \int_{y=e_1}^{e_2} I_e(y) \, E_y^{diff}(y|y_o) dy \, dy_o \tag{14}$$

where $E_y^{dif}(y|y_o)$ is given by (13). Fortunately, the double differentiation in (13) can be removed by integration by parts, giving

$$\Delta Z_{t,e} = - \int_{y_0=t_1}^{t_2} \int_{y=e_1}^{e_2} \frac{I\ell Z_o}{4\pi j} \left[\frac{\sin k(e_2-y) \sin k(t_2-y_o)}{\sin^2 kd} \cdot \right.$$

$$\cdot \frac{-jk}{\rho\rho_o} \cos\frac{\phi}{2} \cos\frac{\phi_o}{2} H_o^{(2)}(kR_1) - \frac{k^2 \cos k(e_2+t_2-y_o-y)}{\sin^2 kd} \pi^{dR}$$

$$\left. + \frac{k^2 \cos k(e_2-t_2-y+y_o)}{\sin^2 kd} \pi^{dR'} \right] dy \, dy_o \tag{15}$$

The expression (15) has been simplified considerably due to the fact that $\pi^{dR}(y|y_o) = \pi^{dR'}(y|y_o)$ if $y=0$ or $y_o=0$, and because PWS modes with a free-space wavenumber were used. Also, (15) does not contain certain terms such as end charges which would cancel when two monopoles are combined to form a dipole. Thus, $[\Delta Z]$ can be calculated with two numerical integrations for (15) and one for (11). These integrations are well behaved, typically requiring only 10-20 Simpson intervals each. This ease of computation of $[\Delta Z]$ is a direct result of the fact that the incident and reflected field components were separated from the total field, allowing

the nearly singular portion, $[Z]_0$, to be evaluated in closed form. Also, Equation (15) is valid for monopole orientations where $e_1 > e_2$ or $t_1 > t_2$, which are required for the complete dipole impedances.

C. Results

The solution described above gave a quickly converging result for the wire currents, as shown in Table I below. This table gives $\Delta Z = Z_{in} - Z_o$, where Z_{in} is the input impedance of a $\lambda/4$, $a = .001\lambda$ monopole near the edge of a half-plane, and Z_o is the input impedance of the same antenna mounted on an infinite ground plane. x_o is the distance of the antenna from the edge. Results are shown for 1, 2, and 3 modes on the monopole. A delta gap generator at the base of the monopole was used.

Table I

X_o/λ	ΔZ, 1 mode	ΔZ, 2 modes	ΔZ, 3 modes
.05	12.1-j7.1Ω	11.8-j8.7Ω	11.7-j9.0Ω
.10	4.2-j8.2Ω	3.5-j9.2Ω	3.3-j9.4Ω
.20	-2.8-j3.8Ω	-3.6-j3.8Ω	-3.7-j3.8Ω
.40	-.32+j1.9Ω	-.09+j2.2Ω	-.04+j2.2Ω
.60	.87-j.73Ω	.85-j.91Ω	.85-j.95Ω

The convergence of Z_o is shown in Table II below:

Table II

Modes	Z_o
1	36.5+j21.1Ω
2	40.6+j20.6Ω
3	41.4+j21.00Ω
4	41.7+j21.3Ω

From the above data it is seen that the solution has practically converged with two wire modes. ΔZ vs x_o is plotted in Figure 7 in Section IIIB, where it is compared with the solution discussed in that section. In Section VB Z_{in} vs x_o is plotted in Figures 11 and 12 and compared with the results of that section. Computation time for this solution is about 30 seconds* when 2 expansion modes are used.

For $x_o = .05$ with two wire modes the impedance matrix elements are

$$[Z_o] = \begin{bmatrix} (23.89-j410.5) & (12.64+j318.5) \\ (12.64+j318.5) & (6.71-j224.1) \end{bmatrix} \Omega$$

$$[Z] = \begin{bmatrix} (2.51-j4.12) & (4.25-j2.38) \\ (4.25-j2.38) & (4.85-j1.67) \end{bmatrix} \Omega \quad .$$

The wire modes are numbered from top to bottom (attachment point).

The solution presented in this section is valid for any distance, x_o, from the half-plane edge except when the antenna is within a few wire radii of the edge. In this case numerical problems are encountered since the fields contain the $1/\sqrt{x}$ edge singularity. The solution presented in Section IV overcomes this difficulty.

D. ϕ-variation of Wire Current

The solution in the previous section used an axial current filament for testing and a circumferentially uniform surface current located on the surface of the wire for expansion. Thus, the solution did not account for or give any information about the circumferential variation of the

---

*All times reported here are for Datacraft 6024 - about 8 times slower than IBM 360/165.

current around the wire surface. This aspect of the solution was of interest for two reasons.

First, it was important to determine if a full account of the circumferential variation of the wire current, due to the edge proximity, would alter the input impedance as determined by the solution in section B, which did not account for any variation. As will be seen, the solution of section B yields the average current on the wire and hence does not change input impedance. Secondly, it was of interest to determine the circumferential variation of the current at the base of the wire in order to build a suitable expansion mode for wires attached near an edge, for use in the surface patch MM solution of Section V.

In this section the solution of section B is extended to allow for the circumferential variation of wire current. This is done by placing expansion filaments spaced evenly around the surface of the wire, i.e., by constructing a wire-grid model of the wire [9]. Each filament is an independent unknown, and can also be broken up into separate modes along its length. Test modes are placed alongside the expansion filaments spaced .000001λ away. This procedure approximates true surface testing and expansion. The solution of section B is then a special case (except for test mode location) of this more general formulation, where only one filament was used.

Figure 3a shows a $\lambda/4$ monopole, radius .001λ, placed .05λ from the edge of a half-plane. Also shown are the positions of eight expansion filaments used in this example. Below is Table III, showing the resulting filament currents at the base of the monopole. In this example 3 modes were employed in the longitudinal direction for a total of 8x3 = 24 unknowns.

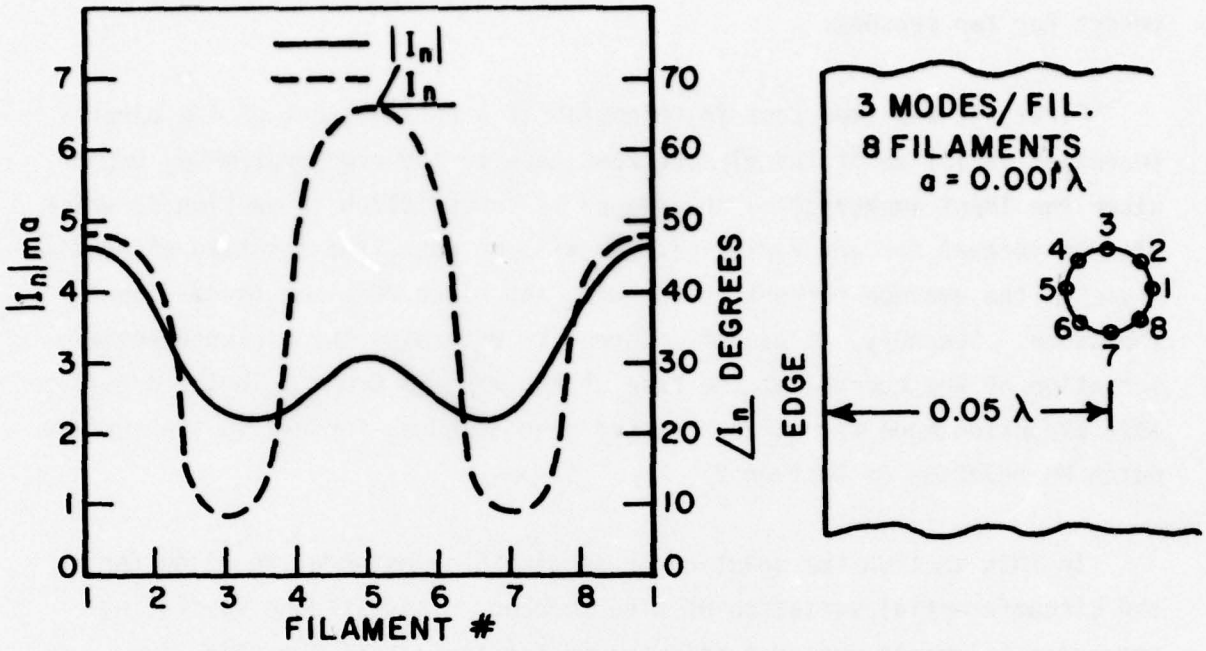

Figure 3. Magnitude and phase of filament current at the base of a monopole .05λ from a half-plane edge, vs. position around the wire. The layout of the eight expansion filaments is also shown.

Table III

Filament #	Current (ma)
1	3.1-j3.4
2	2.9-j2.5
3	2.3-j0.3
4	1.6+j1.9
5	1.2+j2.8
6	1.6+j1.9
7	2.3-j0.3
8	2.9-j2.5

This data is also plotted as magnitude and phase in Figure 3b. As expected, the data show symmetry between filaments 2, 3, 4 and 8, 7, 6, respectively. The data also show, as might be expected, more current flowing away from the edge than toward it. If the filament currents in the above table are added to find the total current, the "average" input impedance can be calculated and is found to be identical to the value given by the simpler one-filament solution of section B. This interesting effect occurs for other segmentation schemes and distances from the edge, and is similar to an effect reported in connection with closely spaced wire antennas [9]. The circumferential variation of the wire current becomes less pronounced as one moves up the wire.

E. Expressions for Surface Currents

In this section simple closed form expressions will be derived for the surface current density on a perfectly conducting half-plane induced by an infinitesimal electric dipole on the surface of the half-plane and near its edge. These results will be used for synthesis of an expansion mode for a wire attachment near an edge in the surface patch MM solution of Section V.

The surface current density on the half-plane is

$$\bar{J}_s = \hat{n} \times \bar{H} \tag{16}$$

For the total surface current density, one must vectorally add the currents on the top of the half-plane ($\phi=0$, $\hat{n}=\hat{y}$) to those on the bottom of the half-plane ($\phi=2\pi$, $\hat{n}=-\hat{y}$):

$$\begin{aligned} J_{sx} &= H_z(\phi=0)-H_z(\phi=2\pi), \\ J_{sz} &= -H_x(\phi=0)+H_x(\phi=2\pi). \end{aligned} \tag{17}$$

Since the dipole is located on the half-plane (top) at $z_o=0$, $\phi_o=0$, so $R=R'$, $\mu_R=\mu_{R'}$, and $I_R=I_{R'}$. Then, from (3) and (4),

$$J_{sx} = \frac{I\ell}{4\pi j}\left\{ - k \left.\frac{\partial I_R}{\partial x_o}\right|_{\phi=0} + k \left.\frac{\partial I_R}{\partial x_o}\right|_{\phi=2\pi}\right\} \tag{18a}$$

$$J_{sz} = \frac{I\ell}{4\pi j}\left\{\frac{-2kz}{R_1\sqrt{\rho\rho_o}} H_1^{(2)}(kR_1) - k \left.\frac{\partial I_R}{\partial z_o}\right|_{\phi=0} + k \left.\frac{\partial I_R}{\partial z_o}\right|_{\phi=2\pi}\right\} \tag{18b}$$

Now let $\alpha=\sinh^{-1}\left\{\frac{2\sqrt{\rho\rho_o}}{R}\right\}$, then

$$\mu_R\Big|_{\phi=0} = \alpha = -\mu_R\Big|_{\phi=2\pi}, \text{ so}$$

$$I_R\Big|_{\phi=0} - I_R\Big|_{\phi=2\pi} = \int_0^{\infty} H_1^{(2)}(kR\cosh u)du + \int_0^{\alpha} H_1^{(2)}(kR\cosh u)du$$

$$- \int_0^{\infty} H_1^{(2)}(kR\cosh u)du + \int_0^{\alpha} H_1^{(2)}(kR\cosh u)du$$

$$= 2\int_0^{\alpha} H_1^{(2)}(kR\cosh u)du \tag{19}$$

$$= 2\psi\,(x,z|x_o,z_o)\big|_{\phi=\phi_o=0}$$

where

$$\psi(x,z|x_o,z_o) = \int_0^{\mu_R} H_1^{(2)}(kR\cosh u)du \tag{20}$$

Then (18) becomes

$$J_{sx} = \frac{I\ell}{4\pi j} \left\{ -2k \frac{\partial}{\partial x_o} \psi(x,z|x_o,z_o) \right\} \tag{21a}$$

$$J_{sz} = \frac{I\ell}{4\pi j} \left\{ -\frac{2kz}{R_1\sqrt{\rho\rho_o}} H_1^{(2)}(kR_1) - 2k \frac{\partial}{\partial z_o} \psi(x,z|x_o,z_o) \right\} \tag{21b}$$

We now develop a small argument approximation for ψ.

For small x,

$$H_1^{(2)}(x) = x/2 + j\frac{2}{\pi x},$$

so (20) becomes

$$\psi \cong \int_0^{\mu_R} \left[\frac{kR \cosh u}{2} + \frac{2j}{\pi kR \cosh u} \right] du$$

$$= k\sqrt{\rho\rho_o} \cos\frac{1}{2}(\phi-\phi_o) + \frac{2j}{\pi kR} \tan^{-1} \frac{2\sqrt{\rho\rho_o}}{R} \cos\frac{1}{2}(\phi-\phi_o) \tag{22}$$

For the present case $\phi=\phi_o=0$, so $\rho=x$ and $\rho_o=x_o$. As a check on the accuracy of this approximation ψ was calculated by numerical integration using (20) and compared with the approximate result in (22). The parameters were $x_o=.05$, $z=0$, $.0075 \leq x \leq .075$, $\lambda=1.$, and the data are listed in Table IV below:

Table IV

x	Exact (Eq. (20))	Approx. (Eq. (22))
.0075	.12+j1.90	.12+j1.76
.0150	.17+j3.20	.17+j2.90
.0225	.21+j4.61	.21+j4.35
.0300	.24+j6.98	.24+j6.68
.0375	.27+j11.91	.27+j11.57
.0450	.29+j31.15	.30+j30.76
.0525	.32+j63.08	.32+j62.67
.0600	.34+j15.39	.34+j14.99
.0675	.36+j8.61	.36+j8.23
.0750	.37+j5.92	.38+j5.55

A similar check was made after ψ was differentiated with respect to x_o. The real part of the approximation to the function ψ is ignored in the remainder of the analysis since it is negligible in comparison to the imagnary part.

The last step is to carry out the differentiations as indicated in (21). When this is done there will be present terms which vary as $1/R^2$. These terms are due to the charges which are located at the ends of the dipole. Since these terms vanish in a physical solution which has continuous current, they are omitted in the final expressions. So, for a vertical electric dipole of moment $I\ell$ near the edge of a half-plane, the surface currents are

$$J_{sx} = \frac{-I\ell}{\pi^2 R_1^2}\left[\sqrt{\frac{x}{x_o}} + \frac{2\sqrt{xx_o}(x-x_o)}{R^2}\right] A/m^2 \tag{23}$$

$$J_{sz} = \frac{-I\ell z}{\pi^2 R_1^2}\left[\frac{1}{\sqrt{xx_o}} + \frac{2\sqrt{xx_o}}{R^2}\right] A/m^2 \tag{24}$$

Observe that $J_{sx} \to 0$ with $\sqrt{x}$ dependence and $J_{sz} \to \infty$ with $1/\sqrt{x}$ dependence, as $x \to 0$ as required by edge conditions. Also, J_{sx} and J_{sz} contain the correct $1/R$ singularity in the vicinity of the source. Identifying this source singular current as J_{sR}, with $\bar{R}$ extending radially outward from the source, gives

$$J_{sR} = \frac{-2I\ell}{\pi^2 R_1^2}\frac{\sqrt{xx_o}}{R} \; A/m^2, \tag{25}$$

with the remainder of the surface current as

$$J_{sx}^{edge} = \frac{-I\ell}{\pi^2 R_1^2}\sqrt{\frac{x}{x_o}} \; A/m^2 \tag{26}$$

$$J_{sz}^{edge} = \frac{-I\ell}{\pi^2 R_1^2}\frac{z}{\sqrt{xx_o}} \; A/m^2 \tag{27}$$

Then J_{sR} contains the source singularity and J_{sx}^{edge} and J_{sz}^{edge} contain the edge terms. Observe that J_{sR} is dependent on circumferential position around the source. It is also of interest to note that Equations (23)-(27) are not frequency dependent, i.e., they are quasi-static results. However, retaining the first term in the real part or higher terms in the imaginary part of (20) will introduce a frequency dependence, if desired. Three-dimensional plots of Equations (23)-(24) are shown in Figures 4 and 5.

Note that the surface currents are unbounded as $x_o \to 0$ (as the source approaches the edge), as might be expected on the basis of reciprocity. However, if the magnitude of the dipole moment is decreased at the same rate as the currents are increasing the final result will be bounded as $x_o \to 0$. This allows an expression for surface current density when an antenna is mounted <u>on</u> the edge. Thus, replacing the dipole moment $I\ell$ by $I\sqrt{\ell x_o}$ in (23) and (24) and letting $x_o \to 0$ gives

$$J_{sx} = \frac{-I}{\pi^2 R_1^2} x \sqrt{\frac{\ell}{x}} \tag{28}$$

$$J_{sz} = \frac{-I}{\pi^2 R_1^2} z \sqrt{\frac{\ell}{x}} \quad , \tag{29}$$

or,

$$J_{sR} = \frac{-I}{\pi^2 R} \sqrt{\frac{\ell}{x}} \ \text{A/m} \tag{30}$$

with $J_{sx}^{edge} = J_{sz}^{edge} = 0$. Equation (30) is the form of the surface current density for a vertical dipole mounted right at the edge of a half-plane. Note the correct source and edge singularties. A 3-D plot of Equation (30) is shown in Figure 6.

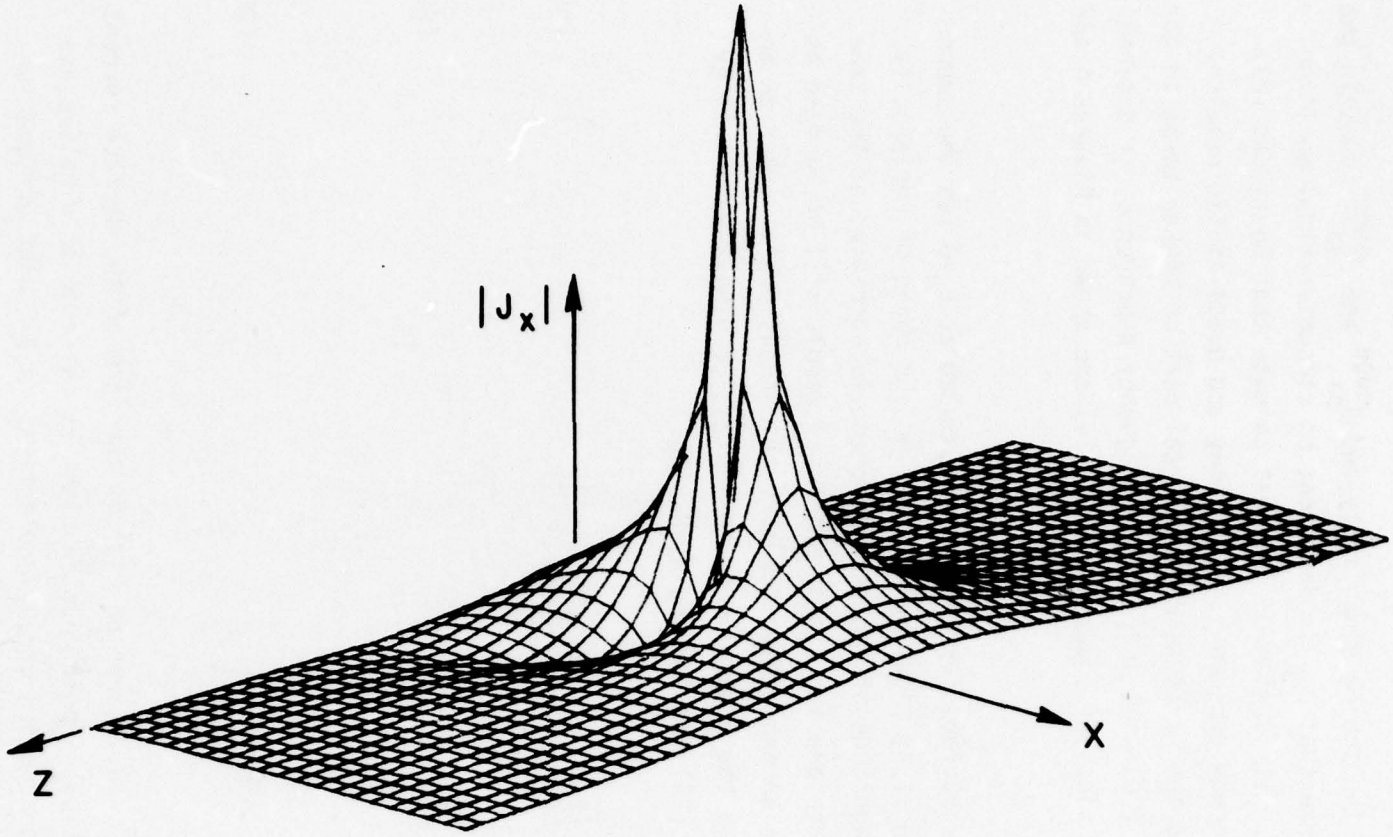

Figure 4. Three-dimensional plot of the magnitude of the surface current density J_{sx} (Equation (28)) for a vertical infinitesimal electric dipole .05λ from the edge of a half-plane. $.001\lambda \leq x \leq 2\lambda$, $-2.5\lambda \leq z \leq 2.5\lambda$.

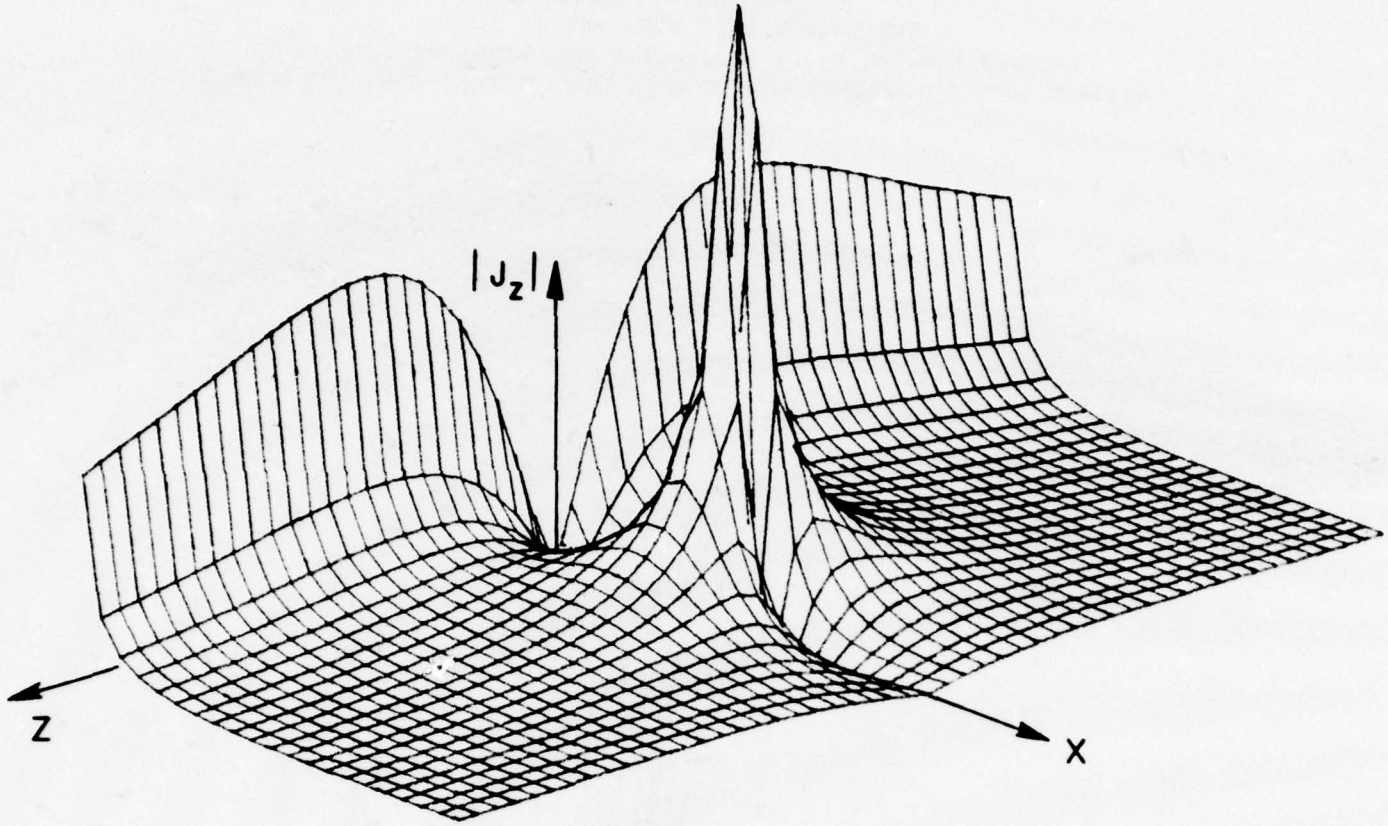

Figure 5. Three-dimensional plot of the magnitude of the surface-current density J_{sz} (Equation (29)) for a vertical infinitesimal electric dipole .05λ from the edge of a half-plane.
$.001\lambda \leq x \leq \lambda$, $-2.5\lambda \leq z \leq .5\lambda$.

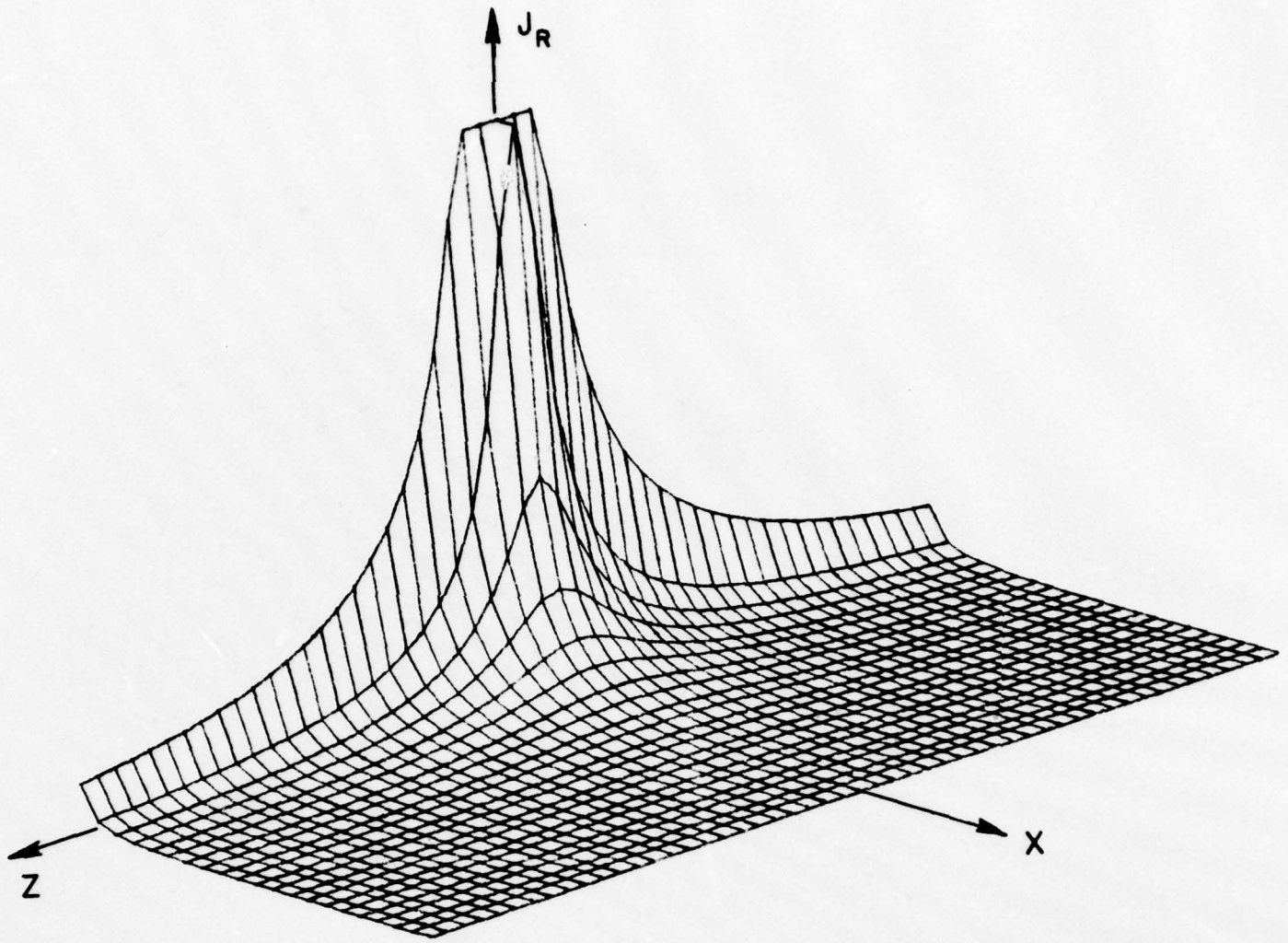

Figure 6. Three-dimensional plot of the surface-current density J_{sR} (Equation (30)) for a vertical infinitesimal electric dipole on the edge of a half-plane. $.001\lambda \leq x \leq 2.\lambda$, $-2.5\lambda \leq z \leq 2.5\lambda$.

III. SOLUTION FOR MONOPOLE NEAR EDGE OF HALF-PLANE USING MM/GTD

A. Formulation of MM/GTD Solution

In this section the solution of section II for a vertical monopole near the edge of a half-plane is repeated using the high frequency or GTD Green's function for the diffracted field rather than the exact Green's function. This type of solution is termed a hybrid MM/GTD solution [2].

The geometrical optics (incident and reflected) terms are separated from the total field and used to compute the $[Z_o]$ matrix, as in section II. The $[Z]$ matrix is computed using (14), except that E_y^{dif} is now calculated using the Kouyoumjian-Pathak GTD formulation for spherical wave incidence [10] (using the notation of [10]):

$$\bar{E}^d(\rho) = \bar{E}^i(Q_E) \cdot \bar{\bar{D}}(\phi,\phi_o,\beta_o')\sqrt{\frac{\rho_o}{\rho(\rho+\rho_o)}}\, e^{-jk\rho}$$

where, for our geometry, $\beta_o' = \pi/2$, $n=2$,

$$\bar{\bar{D}} = \hat{z}\,\hat{z}\,D_s - \hat{\phi}\hat{\phi}D_h,$$

$$L = \frac{\rho\rho_o}{\rho+\rho_o} \quad ,$$

$$\begin{matrix} D_s \\ h \end{matrix} = \frac{-e^{-j\frac{\pi}{4}}}{2\sqrt{2\pi k}\,\sin\beta_o'}\left\{\frac{F(kLa(\phi-\phi_o))}{\cos\left(\frac{\phi-\phi_o}{2}\right)} \mp \frac{F(kLa(\phi+\phi_o))}{\cos\left(\frac{\phi+\phi_o}{2}\right)}\right\},$$

$$a(\beta) = 2\cos^2\beta/2, \quad F(x) = 2j\sqrt{x}\int_{\sqrt{x}}^{\infty} e^{-j\tau^2}\,d\tau.$$

Now, $\bar{E}^i \cdot \hat{z} = 0$, and $E_y = E_\phi \cos\phi$, so

$$E_y^{dif} = -E_t^i(Q_E) \cdot D_h(\phi,\phi_o,\pi/2)\sqrt{\frac{\rho_o}{\rho(\rho+\rho_o)}}\ e^{-jk\rho} \qquad (31)$$

In (31) $E_t^i(Q_E)$ represents the incident electric field evaluated at the half-plane edge which is transverse to the ray path.

Because PWS modes are used this incident field can be expressed in a form very suitable for GTD calculations. In particular, the total exact electric field due to a PWS dipole in free-space can be written as three spherical waves emanating from the middle and endpoints of the dipole[11]. These spherical waves have no ray path field components, making them well suited for use with GTD. Unfortunately, this decomposition is not valid for a PWS monopole, i.e., a ray path field component is necessary to correctly express the field from a PWS monopole. Thus, the incident field from the bottom mode on the wire, being a PWS monopole, is not evaluated exactly. This is a limitation of the present GTD.

B. Comparison of Results from Sections II and III

The input impedance of a $\lambda/4$ vertical monopole versus distance from the edge of a half-plane, computed using MM/Green's function will now be compared to that using MM/GTD. For more resolution, the change in input impedance, ΔZ, from that of a monopole on an infinite ground plane is plotted. That is, $\Delta Z = Z_{in} - Z_o$, where Z_{in} is the input impedance of the monopole on the half-plane and Z_o is the input impedance of the monopole on an infinite ground plane (not to be confused with the $[\Delta Z]$ and $[Z_o]$ matrices). The impedance Z_o and matrix $[Z_o]$ is the same regardless of which method is used.

Figure 7 shows ΔZ vs. d for a $\lambda/4$, a=.004λ monopole with 2 unknowns on the wire. Note that the MM/GTD result agrees well with the exact MM/Green's function result for the monopole as close as .2λ from the edge. The good agreement for distances greater than .2λ gives confidence in the results.

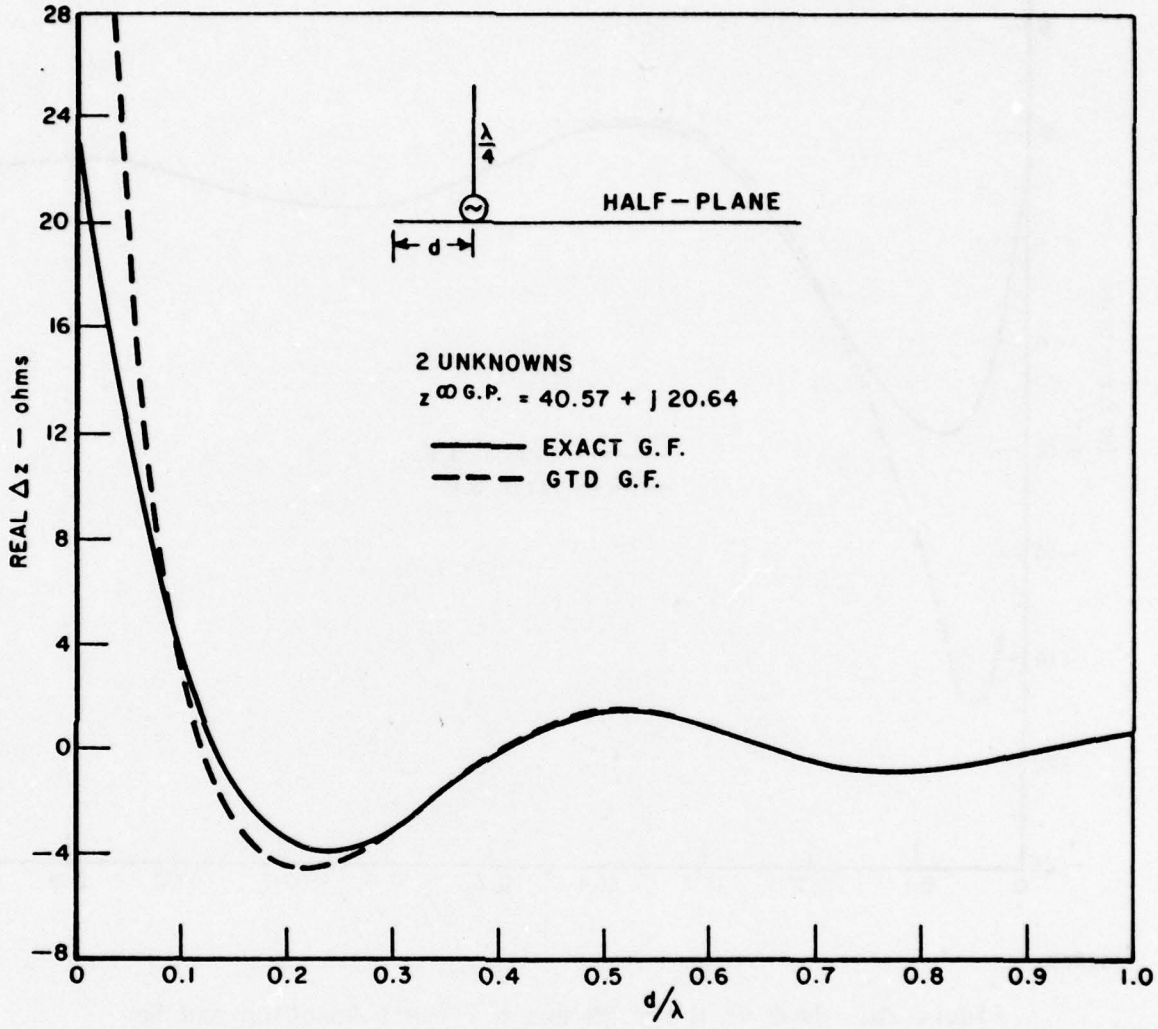

Figure 7a. ReΔZ vs d for MM/exact Green's function and for MM/GTD solutions. ($\Delta Z = Z_{in} - Z_o$, where Z_{in} is the input impedance of the vertical $\lambda/4$ monopole on the half-plane and Z_o is the input impedance of the vertical $\lambda/4$ monopole on an infinite ground plane.)

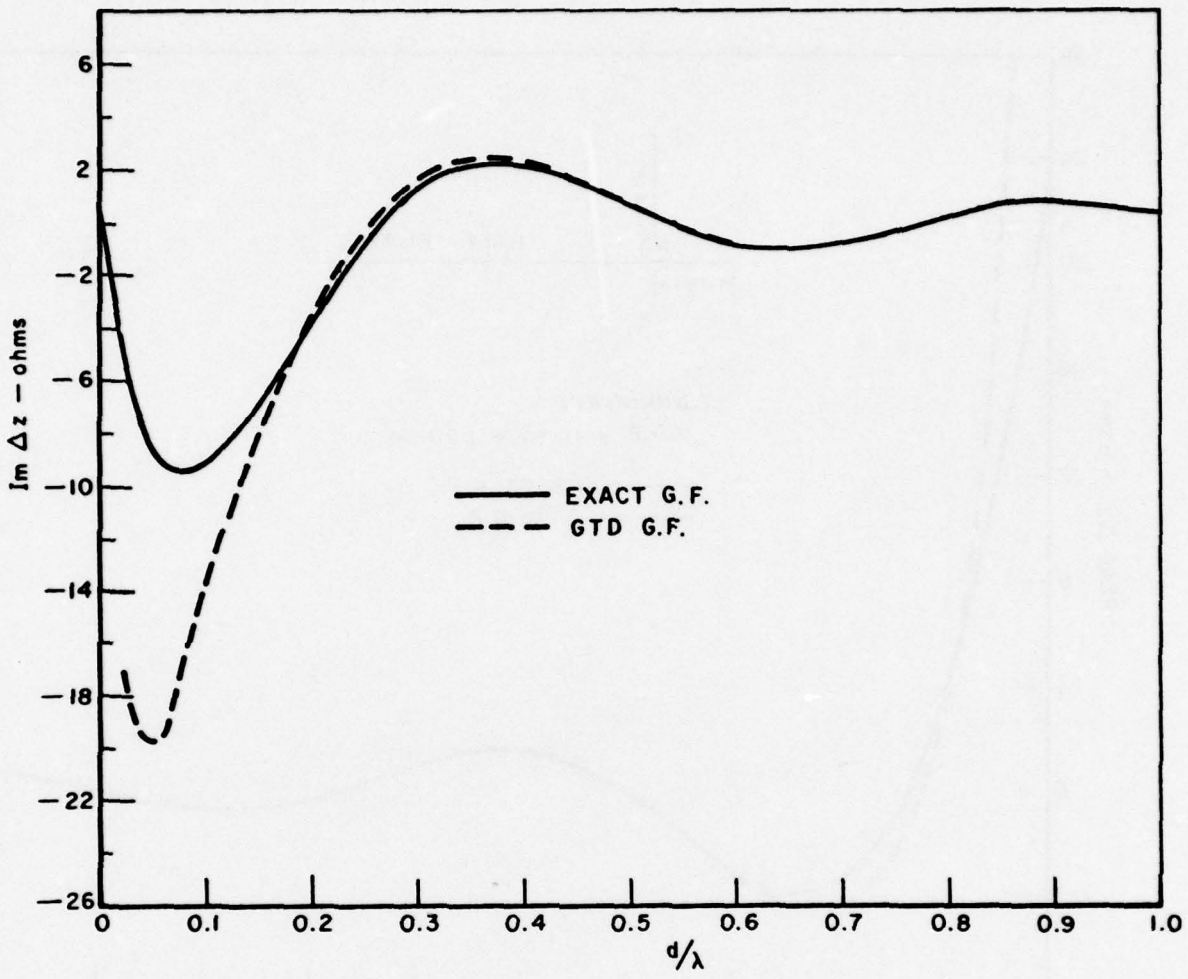

Figure 7b. Im Δz vs d for MM/exact Green's function and for MM/GTD solutions.

As mentioned earlier, the MM/Green's function solution becomes unstable when the monopole is closer than about .002λ from the edges. The curves in Figure 7 were thus extrapolated over this remaining small distance, but compare well with the analysis in Section IV where a rigorous solution is done for a monopole mounted on the edge of a half-plane.

IV. SOLUTION FOR MONOPOLE MOUNTED AT THE EDGE OF A HALF-PLANE USING MM/GREEN'S FUNCTION

A. Formulation of MM/Green's Function Solution

The geometry of the problem is shown in Figure 8. As before, the wire and half-plane are for simplicity taken to be perfectly conducting. The monopole lies in a plane perpendicular to the edge at an angle α from the half-plane surface, connected to the half-plane at the coordinate origin. Without loss of generality, α is restricted to $0 \leq \alpha \leq \pi$.

The solution is similar to that described in Section II, except that here the exact Green's function is expressed in spherical coordinates. The test modes are placed on the wire axis (at $r_o, \theta_o = \frac{\pi}{2}, \phi_o = \alpha, z_o = a$), so the required $\overline{E}$ field component to compute the [Z] matrix is E_{rr} (field in $\hat{r}$ direction due to $\hat{r}$ infinitesimal dipole). Note that, because of the non-zero wire radius, the field along the wire surface, E_ℓ, actually consists of both an E_{rr} and an $E_{\theta r}$ (field in $\hat{\theta}$ direction due to $\hat{r}$ infinitesimal dipole) component: $E_\ell = E_{rr}\left(\frac{\rho}{r}\right) - E_{\theta r}\left(\frac{a}{r}\right)$, where ρ is the cylindrical-coordinate distance of the field point from the edge and a is the wire radius. In the computation of [ΔZ] the $E_{\theta r}$ term is ignored, which is probably justifield whenever the field point is ten wire radii or more from the edge (then $a/r \ll 1$). It is felt however, that ignoring this term has a small but noticeable effect on the input impedance, in particular on the imaginary part. The reason that this $E_{\theta r}$ component was not included in the analysis was that it was too difficult to do so. The results given in the next section show that this approximation is justified.

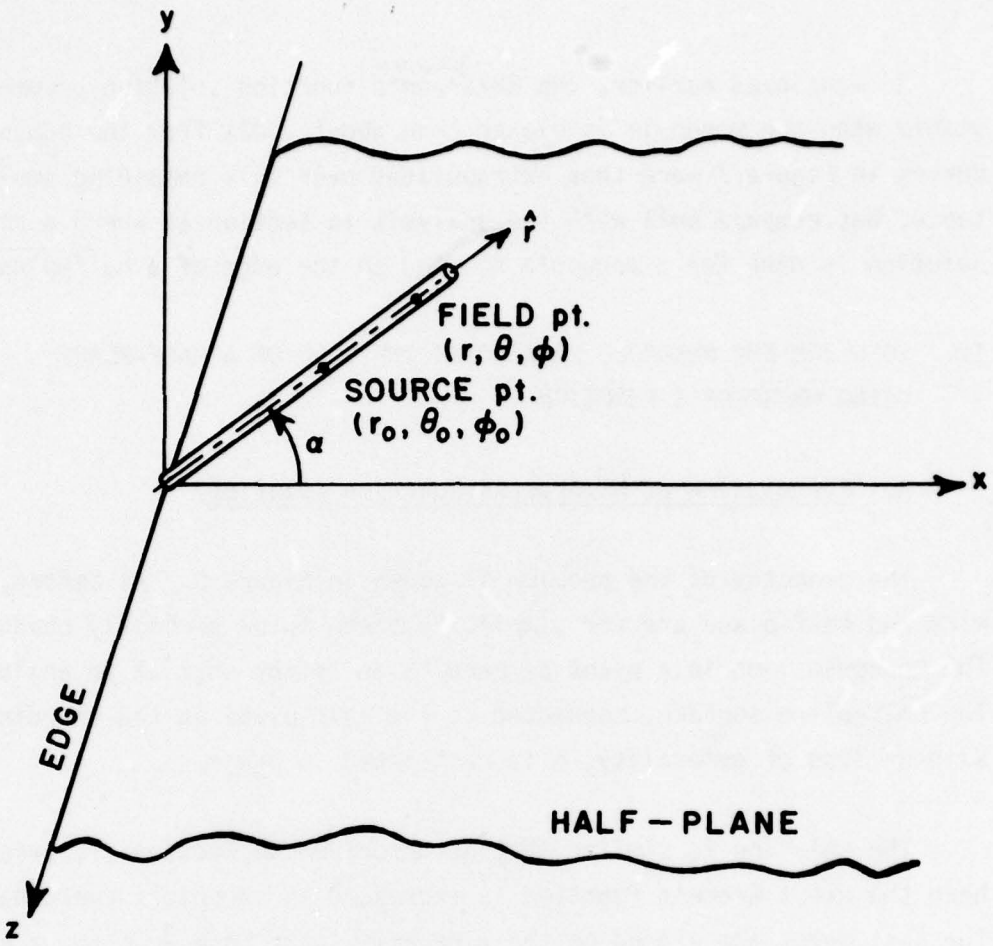

Figure 8. Geometry and coordinate system for a monopole mounted at the edge of a half-plane.

From another paper by Senior[12], the radial component of the electric field due to a radially directed electric dipole, with moment $I\ell$, near the edge of a half-plane is

$$E_{rr} = \frac{I\ell Z_o}{4\pi j} \left\{ \frac{-j}{2} \left(\frac{\partial^2}{\partial r_o^2} + k^2 \right) \frac{r_o}{r} \left(I_R - I_{R'} \right) \right\}, \tag{32}$$

The magnetic field components tangential to the half-plane, for use later in determining the surface current, are

$$H_{\theta r} = \frac{I\ell Z_o}{4\pi j}\left\{\frac{j\omega\varepsilon}{r\sin\theta}\left(\frac{-j}{2}\right)\frac{\partial}{\partial\phi}\frac{r}{r_o}\left(I_R - I_{R'}\right)\right\} \quad , \tag{33}$$

$$H_{rr} = 0 \quad ,$$

where I_R and $I_{R'}$ are defined in (5). Equations (32), (33) represent the fields in terms of a Debye potential, whereas Equations (2)-(4) represented the fields in terms of a Hertz potential.

Now, it can be shown that

$$E_{rr}^{inc} = \frac{I\ell Z_o}{4\pi j}\left\{\left(\frac{\partial^2}{\partial r_o^2} + k^2\right)\frac{r_o}{r}\,\frac{e^{-jkR}}{kR}\right\}, \text{ and} \tag{34}$$

$$E_{rr}^{image} = -\frac{I\ell Z_o}{4\pi j}\left\{\left(\frac{\partial^2}{\partial r_o^2} + k^2\right)\frac{r_o}{r}\,\frac{e^{-jkR'}}{kR'}\right\} \quad , \tag{35}$$

where the minus sign in (35) is due to the fact that the image dipole is in the $-\hat{r}$ direction. Then, defining

$$E_{rr} = E_{rr}^{inc} + E_{rr}^{image} + E_{rr}^{dif} \quad , \tag{36}$$

we have

$$E_{rr}^{dif} = \frac{I\ell Z_o}{4\pi j}\left\{\left(\frac{\partial^2}{\partial r_o^2} + k^2\right)\frac{r_o}{r}\left(\pi^{dR} - \pi^{dR'}\right)\right\} \tag{37}$$

where π^{dR} and $\pi^{dR'}$ are defined in (10) or (11). Observe that when $\alpha>\pi/2$ there is no reflected E_{rr} field for $\phi>\pi/2$, so (37) does not strictly represent the diffracted field in the usual sense.

The source and image fields are then separated from the total field, and the $[Z_o]$ section of the total impedance matrix [Z] is computed in closed form as before, using Richmond's subroutines [8]. The $[\Delta Z]$ elements are found by

$$\Delta Z_{ij} = - \int_{r_{oi}} \int_{r_j} I_i(r_o) E^{dif}_{rr} (r|r_o) I_j(r) dr\, dr_o, \tag{38}$$

where r_{oi} ranges over the test mode and r_j ranges over the expansion mode. The differentiations in (37) can be eliminated by integration by parts. If we let $K(r|r_o) = \frac{r_o}{r}(I_R - I_{R'})$, much simplification is possible by noting that $K(r|0)=0$, $\frac{\partial}{\partial r_o} K(r|r_o)|_{r_o=0}=0$, and $\frac{\partial^2}{\partial r^2} I(r) = -k^2 I(r) - 2k\cot kd\,\delta(r-r^m)$ for $I(r)$ being the current of a PWS dipole and r^m the midpoint (terminal point) of the dipole. The final form after simplification is

$$\Delta Z_{ij} = \frac{-k}{\sin kd} \cdot \frac{I\ell Z_o}{4\pi j} \int_{r_j} I_j(r) \left[K(r|r^t_{oi}) + K(r|r^b_{oi}) - 2\cos kd\, K(r|r^m_{oi})\right] dr, \tag{39}$$

where r^t_{oi}, r^m_{oi}, r^b_{oi} are the radial coordinates of the top, middle, bottom, respectively of the i-th test dipole. If the test mode is the bottom mode, which is a monopole, then $r^m_{oi} = r^b_{oi} = 0$. d is the length of the mode segments.

This solution was programmed and run for a $\lambda/4$, a=.001λ monopole, with a delta gap generator at the base of the monopole, vs angle α.

Below are shown the ΔZ_{ij} elements with two wire modes and $\alpha=\pi/2$. The $[Z_o]$ matrix is identical to that given in Section II. The expansion modes are numbered from top to bottom (attachment point) as before.

$$[\Delta Z] = \begin{bmatrix} (.75-j9.56) & (7.45+j5.03) \\ (7.43-j24.29) & (13.38+j23.88) \end{bmatrix} \Omega$$

The asymmetry in the $[\Delta Z]$ matrix is attributed to the fact that the $E_{\theta r}$ field component was neglected, and possibly because full surface testing and expansion was not used. However, the $[\Delta Z]$ elements are relatively small compared to the $[Z_o]$ elements (see section IIC) reducing the final error.

Figure 13 shows Z_{in} using two modes on the wire compared with the surface patch MM solution. This result at $\alpha=\pi/2$ also agrees with the analysis for the vertical monopole in Section II as x_o approaches zero. Note that Z_{in} goes to zero as α approaches zero as expected, since the antenna then becomes shorted by the ground plane. As α approaches zero, the reactance curve takes a sharp turn downward before going to zero. This effect is probably explained by the fact that the capacitance between the monopole and half-plane increases sharply as the monopole gets closer to the half-plane, before going to zero as it touches the half-plane.

Another independent check is available from Tai [5] who computed the input resistance of a monopole at $\alpha=\pi$ by integrating the far field radiation pattern. Tai obtained, using one mode on the wire, a value of 86.3Ω while our analysis, using one mode, gives 85.2Ω for the input resistance (the input reactance cannot be calculated using Tai's method). Also shown in Figure 13 is a surface patch result obtained by Glisson [13] for a $\lambda/4$ monopole mounted on the edge of a finite plate, which compares reasonably with the other results.

B. Expression for Surface Current

In this section a simple closed form expression is derived for the surface current density on a perfectly conducting half-plane induced by an infinitesimal electric dipole mounted at the edge. The surface current density on the half-plane is $\bar{J}_s = \hat{n} \times \bar{H}$. Since $\hat{n} = \pm\hat{\phi}$ and $H_{rr} = 0$ the only surface current component is $J_{sr} = -H_{\theta r}(\phi=0)+H_{\theta r}(\phi=2\pi)$, which is the sum of the surface currents on the top and bottom of the half-plane. As expected, the entire surface current flows radially outward from the dipole. Then, using (33),

$$J_{sr} = \frac{-\omega\epsilon}{2r_o \sin\theta} \quad \frac{I\ell Z_o}{4\pi j} \quad \frac{\partial}{\partial\phi} \left[(I_R - I_{R'})\big|_{\phi=0} - (I_R - I_{R'})\big|_{\phi=2\pi}\right] \tag{40}$$

Now, $R(\phi=0)=R(\phi=2\pi)$ and $\left.\frac{\partial R}{\partial \phi}\right|_{\phi=0} = \left.\frac{\partial R}{\partial \phi}\right|_{\phi=2\pi}$, so the $\int_o^\infty (\quad)$ part of the integrals in I_R and $I_{R'}$ of (5) cancel, since they are only functions of R or R'. Also, it can be shown that the remaining terms can be written as

$$J_{sr} = \frac{-2\omega\epsilon}{r_o \sin\theta} \frac{I\ell Z_o}{4\pi j} \left.\frac{\partial \psi}{\partial \phi}\right|_{\phi=0}, \tag{41}$$

where ψ is defined in (20). Then, using the small argument approximation given in (22),

$$J_{sr} = \frac{-4j\omega\epsilon}{\pi k r_o \sin\theta} \frac{I\ell Z_o}{4\pi j} \frac{\partial}{\partial \phi}\left(\frac{1}{R} \tan^{-1}\left[\frac{2\sqrt{\rho\rho_o}}{R} \cos\tfrac{1}{2}(\phi-\phi_o)\right]\right)_{\phi=0} \tag{42}$$

Carrying out the differentiation and ignoring terms of order $1/R^2$, which account for end charges, gives

$$J_{sr} = \frac{-4j\omega\epsilon}{\pi k r_o \sin\theta} \frac{I\ell Z_o}{4\pi j} \frac{1}{R_1^2}\left[\frac{2rr_o\sqrt{\rho\rho_o}}{R^2} \cos\frac{\phi_o}{2} \sin\phi_o \sin\theta + \sqrt{\rho\rho_o} \sin\frac{\phi_o}{2}\right]. \tag{43}$$

Up to this point the infinitesimal dipole has been located at ($r_o \neq 0$, $\theta_o=\pi/2, \phi_o$). To move the dipole to the edge ($r_o \to 0$) the dipole moment must be reduced as $\sqrt{r_o}$, as was done in Section II, to maintain finite fields. Thus, for a dipole of moment $I\sqrt{\ell r_o}$ at the edge, the surface current density is ($R_1=r$ at $r_o=0$)

$$J_{sr} = \frac{-I\sqrt{\ell\rho}}{\pi^2 \sin\theta} \frac{1}{r^2} \sin\frac{\phi_o}{2}, \text{ or, since } \sin\theta = \rho/r = x/r,$$

$$J_{sr} = \frac{-I}{\pi^2}\sqrt{\frac{\ell}{x}} \cdot \frac{1}{r} \sin\frac{\phi_o}{2} \text{ A/m} \tag{44}$$

For a vertical dipole, $\phi_o=\pi/2$, giving

$$J_{sr} = \frac{-I}{\pi^2}\sqrt{\frac{\ell}{x}}\ \frac{1}{r}\ \frac{1}{\sqrt{2}}\ \text{A/m.} \qquad (45)$$

Equation (45) agrees in form with result (30) in Section II but differs by a factor of $\sqrt{2}$. The reason for this discrepancy is not known at present, but probably has something to do with the strength of the dipole moment. For this work, we are primarily interested in the <u>form</u> of the current. Observe that Equations (44)-(45) have the proper source and edge singularities, and that the orientation angle of the dipole, ϕ_o, does not affect the form of the current density.

Glisson [13] derived a similar result for the surface currents induced by a radial source mounted on the edge of a wedge of arbitrary angle. For the case of a half-plane his result reduces to $J_r \sim \frac{1}{\sqrt{xr}}$, which disagrees with the form of our result in terms of the source singularity. It is felt that Glisson's solution does not predict the correct source behavior because his solution was based on retaining only the first term in an eigenfunction expansion. As mentioned previously, this procedure usually predicts the correct edge behavior but not the correct source behavior.

V. SURFACE PATCH MM SOLUTION

This section deals with methods of modifying the author's surface patch modelling program [4] to handle antennas mounted near or at the edge of plates. Originally, the program used an attachment mode which had the following features:

a) enforced continuity of current from wire to plate.

b) enforced the proper $\hat{\rho}/\rho$ dependence for surface current in the vincinity of the attachment point.

c) had no ϕ-variation in surface current. (In this section ϕ is used to denote azimuthal direction around the attached wire.)

d) worked well for wire attachments .1λ or further from an edge.

This attachment mode, shown in Figure 9a, failed for antennas mounted closer than .1λ from the edge as shown in Figures 11 and 12, probably for the following reasons:

a) disk mode radius was limited to the distance of the monopole from the edge, thus reducing the area in which the $\hat{\rho}/\rho$ singularity was enforced.

b) disk mode did not contain any ϕ-variation in current density, which probably becomes increasingly important as the antenna gets closer to the edge.

c) for small distances from the edge, the current filaments constituting the disk mode are very short, making calculation of mutual impedances difficult.

Thus, a better attachment mode was needed to handle antennas mounted close to or at the edge of plates.

A. Description of Attachment Mode Development

All of the attachment modes that were developed consisted of a disk section which rested on the plate structure, and a vertical wire monopole with terminals at the center of the disk. Since this wire monopole was common to all attachment modes, it is not described in detail here.

Mode A) The original disk monopole part of the attachment mode had surface current density [4]

$$J_\rho(\rho) = \frac{\sin k(b-\rho)}{2\pi\rho \sin k(b-a)} , \qquad (46)$$

where a is the wire radius and b is the outer radius of the disk, usually taken to be between 0.1λ and 0.25λ, if room permits (see Figure 3 of [4]). Figure 9a shows how this mode would be applied to a wire attachment near an edge.

Mode B) The first approach toward improvement of the disk mode A) was to maintain the disk radius at about $.2\lambda$ where it overlapped the plate, but cut off the disk where it overhung the plate, see Figure 9b. The surface current density for this disk mode can be written as

$$J_\rho(\rho,\phi) = B \frac{\sin k(b(\phi)-\rho)}{2\pi\rho} \quad , \tag{47}$$

where B is a constant chosen for unit terminal current, i.e.,

$$\int_{\phi=0}^{2\pi} J_\rho(a,\phi)\,a\,d\phi = 1A, \tag{48}$$

and $b(\phi)$ is the outer radius of the disk mode, now expressed as a non-constant function of ϕ.

This type of mode overcomes some of the drawbacks of the previous mode in that it has a ϕ-variation of current and yields a larger area where the $1/\rho$ singularity is enforced. The results obtained when using this mode are not significantly better than those obtained with the original mode A). This is probably due to the fact that the ϕ-dependence is not close enough to the exact dependence. For instance, when ρ is close to a, the current density of mode B) is large but does not vary appreciably with ϕ, while the analysis of Section II, Equation (25), shows that significantly less current is flowing toward the edge than away from it. Another point is that this mode does not have a uniform limit as the attachment point approaches the edge. One would expect that the current flowing toward the edge would smoothly decrease to zero as the attachment moves to the edge. Mode B) does not have this behavior. The disk modes presented below do have this desired asymmetry.

Mode C) The next step was to construct a disk mode which had less current flowing toward the edge than away from it. One distribution which does this is

$$J_\rho(\rho,\phi) = C \frac{\sin k(b(\phi)-\rho)}{2\pi\rho} \sin kb(\phi), \tag{49}$$

where C is a constant chosen to satisfy (48). This current distribution roughly corresponds to that obtained from the exact solution for the circumferential current variation, as shown in Figure 3b. This type of mode has the desired property of uniformly approaching a semi-circular disk as the attachment point moves to the edge (Figure 9c). Also, this mode reduces to the standard attachment mode, mode A), when the distance between the attachment point and edge becomes greater than the disk outer radius ($\sim.2\lambda$), since $b(\phi)$ = constant for this case.

This type of attachment mode gave the best results for antennas at or near an edge. These results are compared with others later.

Mode D) The next type of disk mode which was developed was one constructed from an arbitrary number of wedge-shaped sectors of current, with current distribution like that of disk mode B) over each sector, but with each sector being an independent unknown. See Figure 10, which shows a 4 sector disk. This type of mode has the advantage of allowing the MM solution to arrive at currents (both magnitude and phase) which best satisfy the integral equation in a least mean square sense. The resolution of the variation in disk current can be made finer by increasing the number of wedge-shaped sectors that the disk is broken into. When eight such sectors were used the results for input impedance agreed fairly well with those obtained using mode C). The resulting sector currents for $x_o=.05\lambda$, $a=.001\lambda$, and 8 sectors with sector 1 oriented directly away from the edge are given in Table V below:

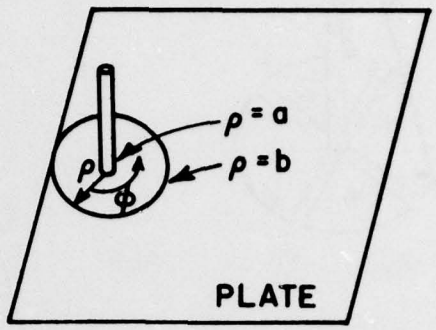

a) original attachment mode, mode A)

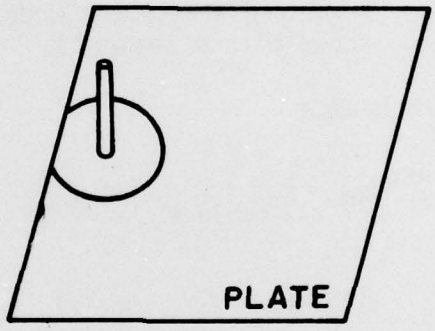

b) final attachment mode, mode C)

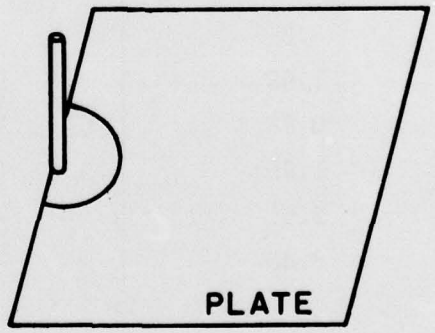

c) attachment mode C) when monopole is mounted at a plate edge.

Figure 9.

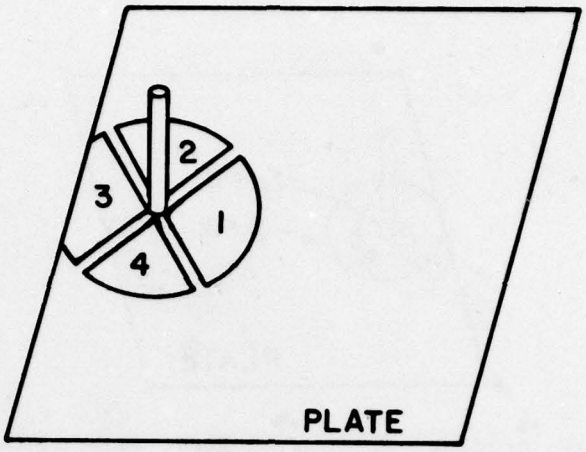

Figure 10. Segmented attachment mode, mode D), shown with 4 segments.

Table V

Sector	$\lvert I_n \rvert$ (ma)	$\angle I_n$ (deg.)
1	4.61	-2
2	3.44	-16.
3	3.35	-8.
4	1.98	12
5	0.68	1.
6	1.95	11.
7	3.61	-7.
8	3.30	-16.

Note the symmetry between sectors (4,6), (3,7) and (2,8); the symmetry is not exact probably because of numerical integration error. This current distribution is similar in magnitude to that shown in Figure 3b, but not in phase. This is interesting, because it implies that the enforcement of the proper phase variation is not crucial to a correct result for input impedance. This could explain why mode C), which enforces current magnitude but not phase, gives good results.

Edge Mode:

Recently, there has been an interest in directly enforcing the edge condition in MM solutions [14]. Thus, it was decided to construct a mode, based on the analysis of Section IIE, that would enforce the edge singularity of the surface current component parallel to the edge of the half-plane, and study its effect on the solution. This "edge mode" was constructed from PWS current filaments to embody the essential features of Equation (27). The surface current density of this mode is

$$J_s(x,z) = \frac{A}{\sqrt{x}} \begin{cases} \dfrac{-\sin k(z+\ell)}{\sin k(\ell-z_o)} & \text{for } -\ell<z<-z_o, \\ \dfrac{\sin kz}{\sin kz_o} & \text{for } -z_o<z<z_o \\ \dfrac{\sin k(z-\ell)}{\sin k(z_o-\ell)} & \text{for } z_o<z<\ell \end{cases} \tag{50}$$

where the coordinate system is shown in Figure 1, A is a suitable normalizing constant, and 2ℓ is the overall length of the mode. The width of the mode (extent in x-direction) is arbitrary, but since most of the current is located near the singularity at x=0, this width is not too critical if chosen to be $.05\lambda$ or greater. The result of using this edge mode with different lengths and widths was interesting. First, the edge mode was excited in the surface patch MM solution, as indicated by a non-zero mode current. However, the input impedance did not significantly change from the result obtained without using an edge mode. Thus, all of the other surface patch, wire, and attachment currents changed in the presence of

the edge mode in such a way as to leave the input impedance unaltered. At the present time the best explanation we have for this effect is that the singular behavior of the edge current can be approximated adequately in a least-mean-square sense by the surface-patch dipoles alone. Incorporation of a special edge mode explicitly satisfying the edge condition does not improve on this situation in the present case.

B. Results and Comparisons with Solutions from Sections II, III, IV

In this section results from other sections are compared with the surface patch MM results. Of necessity, the surface patch MM solution must be based on a finite size plate rather than a semi-infinite half-plane. For this reason it is more appropriate to plot Z_{in} rather than ΔZ. Also, the size of this finite ground plane can have some effect on the input impedance, as shown in Table VI below which gives the input impedance of a $\lambda/4$ monopole $.05\lambda$ away from the long edge of different sized ground planes.

Table VI

Plate Size	Z_{in} (Ω)
.4 x.5λ	44.+j13.
.8 x1.λ	71.+j12.
.8 x1.2λ	54.-j4.6
.8x1.5λ	42+j12.

This variation seems to be a plate resonance effect, and probably explains the offset of a few ohms between the surface patch MM and other solutions in the following figures.

Figures 11 and 12 show the real and imaginary parts of the input impedance of a $\lambda/4$, $a=.001\lambda$ monopole at a distance d from the edge of a half-plane, as calculated with the exact MM/Green's function solution (Section

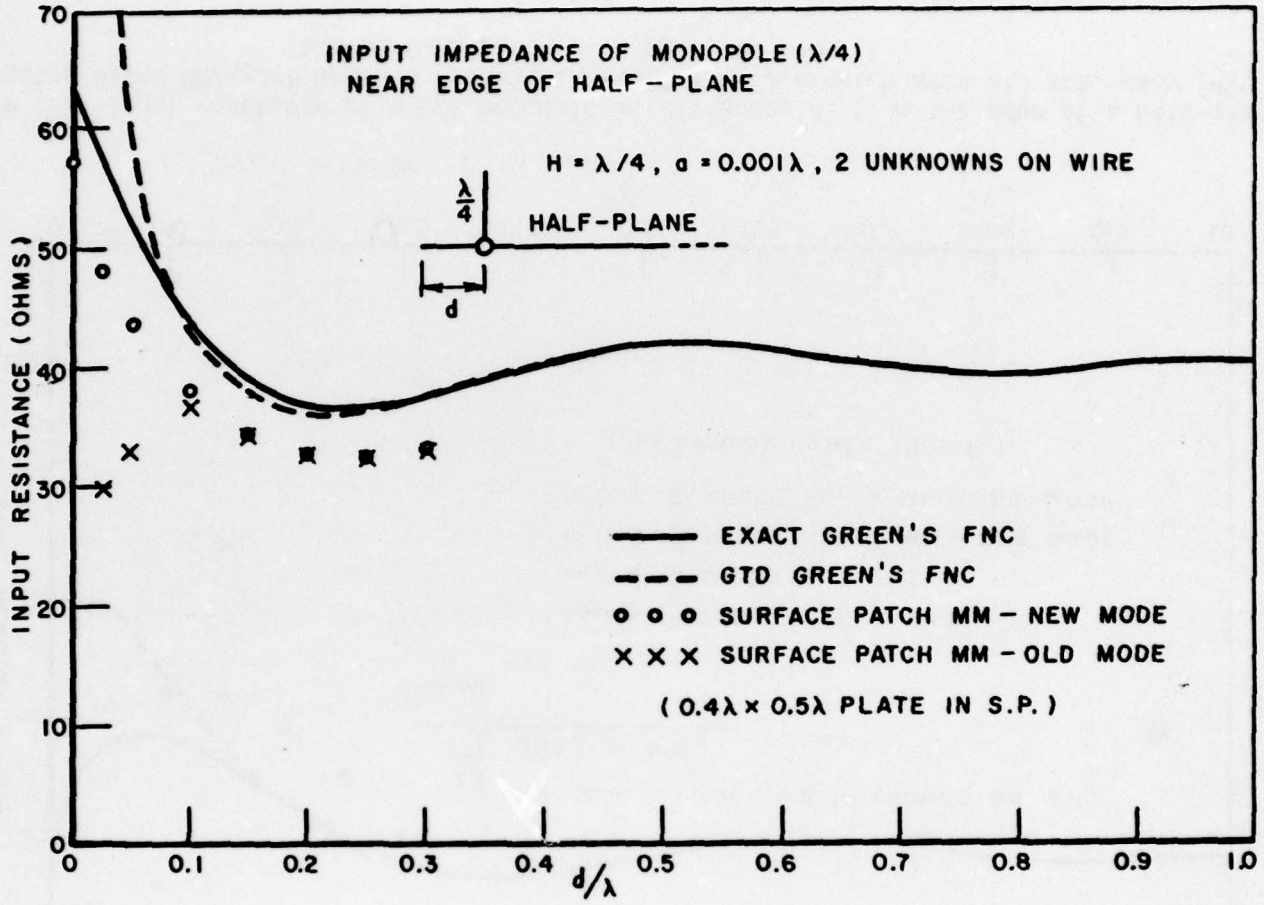

Figure 11. Input resistance of a λ/4 monopole vs distance, d, from the edge of a half-plane computed using MM/exact Green's function, MM/GTD, surface patch with old att. mode (A), and surface patch with new att. mode (C).

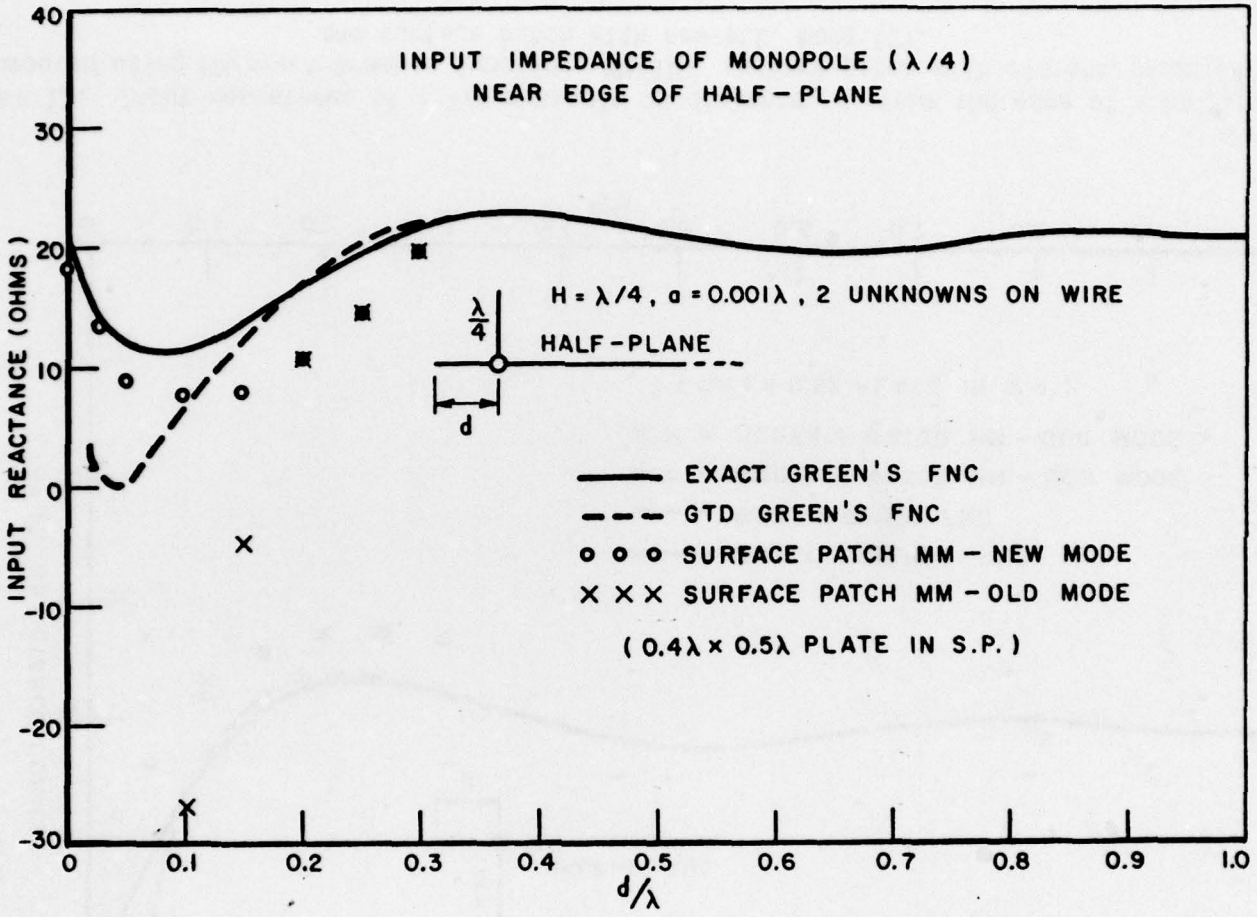

Figure 12. Input reactance of a λ/4 monopole vs distance, d, from the edge of a half-plane computed using MM/exact Green's function, MM/GTD, surface patch with old att. mode (A), and surface patch with new att. mode (C).

II), the MM/GTD solution (Section III), and the surface patch MM solution using mode A) and mode C). Remember that the surface patch MM results are for finite ground planes, in this case .4λx.5λ, with 7 plate modes, 1 attachment mode, and 1 wire mode. The solutions of Sections II and III both used 2 modes on the wire monopole. From these graphs it can be seen that the original surface patch attachment mode does indeed fail when the antenna is chosen closer than .1λ to the edge, and that the modified attachment mode (mode C) performs much better. Recall that the offset of the surface patch results from the other curves can be accounted for by the finite plate size required for the surface patch result.

Figure 13 presents the results for a λ/4, a=.001λ monopole mounted at the edge of a half-plane vs angle based on the solution discussed in Section IV, and compared with the surface patch MM solution with attachment mode C). Discussion of the solution of Section IV and comparison with independent results was given in Section IV. The surface patch MM result in Figure 13 used a semicircular attachment mode like that shown in Figure 9c, with a .4λx.5λ plate and 9 modes total.

VI. CONCLUSION

This report has presented analysis and results of the problem of a monopole antenna mounted near or at the edge of a half-plane or plate. The canonical solutions using exact Green's functions have been presented as a basis for comparison with other solutions. Expressions for near-zone surface current density were derived and used to synthesize an attachment mode to handle wire attachments near plate edges in a general surface patch MM solution.

The most obvious extension of the work presented here would be the analysis of monopoles mounted near or on the edge of a wedge of arbitrary angle. The handling of wedges in the canonical solutions would be more difficult than that for half-planes because the Green's function for a wedge is not in as convenient a form as is the half-plane Green's function.

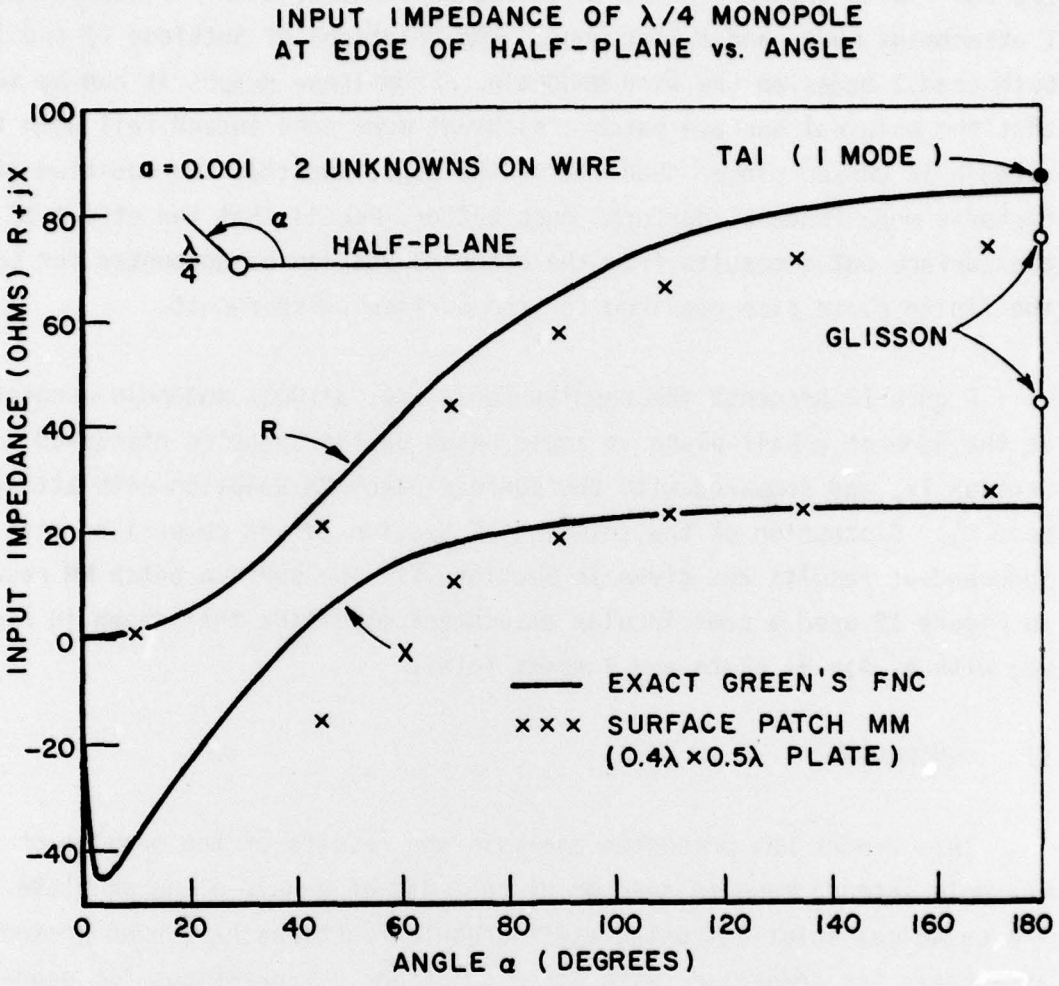

Figure 13. Input impedance of a λ/4 radial monopole mounted at the edge of a half-plane vs. angle, computed using MM/exact Green's function and surface patch with att. mode (C). Also shown are independent results for R and Z at $\alpha=180^{0}$, from Tai and Glisson, respectively.

However, the surface patch solution for antennas would probably be easier, for two reasons. First, the half-plane represents the "worst case" as far as edge effect. That is, a wedge with interior angle greater than zero would be expected to have less effect on input impedance than would a half-plane. Second, the surface current flow around the edge of a wedge can probably be handled with surface patch modes and minor modifications to the attachment mode.

Another related area for future work would be the case of a monopole mounted near a corner or vertex. Also, these solutions could be extended to account for mutual coupling between two or more antennas near edges in a straightforward manner.

REFERENCES

1. F. M. Tesche and A. R. Neureuther, "The Analysis of Monopole Antennas Located on a Spherical Vehicle," IEEE-EMC-18, pp. 2-15, February 1976.

2. G. A. Thiele and T. H. Newhouse, "A Hybrid Technique for Combining Moment Methods with the Geometrical Theory of Diffraction," IEEE-AP-23, January 1975.

3. N. C. Albertsen, J. E. Hansen and N. E. Jensen, "Computation of Radiation from Wire Antennas on Conducting Bodies," IEEE-AP-22, pp. 200-206, March 1974.

4. E. H. Newman and D. M. Pozar, "Electromagnetic Modelling of Composite Wire and Surface Geometries," IEEE AP-26, pp. 784-789, November 1978.

5. C. T. Tai, "Dyadic Green's Functions in Electromagnetic Theory," Intext, Scranton, Pa., 1971, pp. 123-165.

6. Y. T. Lin and J. H. Richmond, "EM Modelling of Aircraft at Low Frequencies," IEEE AP-23, pp. 53-56, January 1975.

7. T. B. A. Senior, "The Diffraction of a Dipole Field by a Perfectly Conducting Half-Plane," Quart. Journ. Mech. and Applied Math., Vol. VI, Pt. 1, 1953.

8. J. H. Richmond, "Computer Program for Thin-Wire Structures in a Homogeneous Conducting Medium," Report 2902-12, August 1973, The Ohio State University ElectroScience Laboratory, Department of Electrical Engineering; prepared under Grant NGL 36-008-138 for National Aeronautics and Space Administration. (NASA-CR-2399)

9. P. Tulyathan and E. H. Newman, "The Circumferential Variation of the Axial Component of Current in Closely Spaced Thin-Wire Antennas," IEEE AP-27, pp. 46-50, January 1979.

10. R. G. Kouyoumjian and P. H. Pathak, "A Uniform Geometrical Theory of Diffraction for an Edge in a Perfectly Conducting Surface," IEEE Proceedings, November 1974, pp. 1448-1461.

11. E. P. Ekelman and G. A. Thiele, "A Hybrid Technique for Combining the Moment Method Treatment of Wire Antennas with the GTD for Curved Surfaces," Report 784372-5, July 1978, The Ohio State University Electro-Science Laboratory, Department of Electrical Engineering; prepared under Contract N00014-76-C-0573 for Office of Naval Research, pp. 48-55. OAD/A058495)

12. J. J. Bowman and T. B. A. Senior, "Diffraction of a Dipole Field by a Perfectly Conducting Half-Plane," Radio Science, vol. 2, No. 11, November, 1967, pp. 1339-1345.

13. A. W. Glisson, "On the Development of Numerical Techniques for Treating Arbitrarily-shaped Surfaces," Dissertation, University of Mississippi, June 1978.

14. D. R. Wilton and S. Govind, "Incorporation of Edge Conditions in Moment Method Solutions," IEEE AP-25, No. 6, November 1977.